Supramolecular Engineering of Non-planar Bridged-Ethers: Blue to Red Emission Tuning and Solution-Processed OLED Fabrication

Shouvik Bhuin[1,2], Upasana Deori[2], Pandiyan Sivasakthi[1], Avanigadda Madhu Niharika[1], Pralok K. Samanta[1], Pachaiyappan Rajamalli*[2] and Manab Chakravarty*[1]

[1]Department of Chemistry, BITS-Pilani Hyderabad Campus, Hyderabad-500078, India, [2]Materials Research Centre (MRC), Indian Institute of Science (IISc) Bangalore 560012, India

Synthetic routes and characterization details

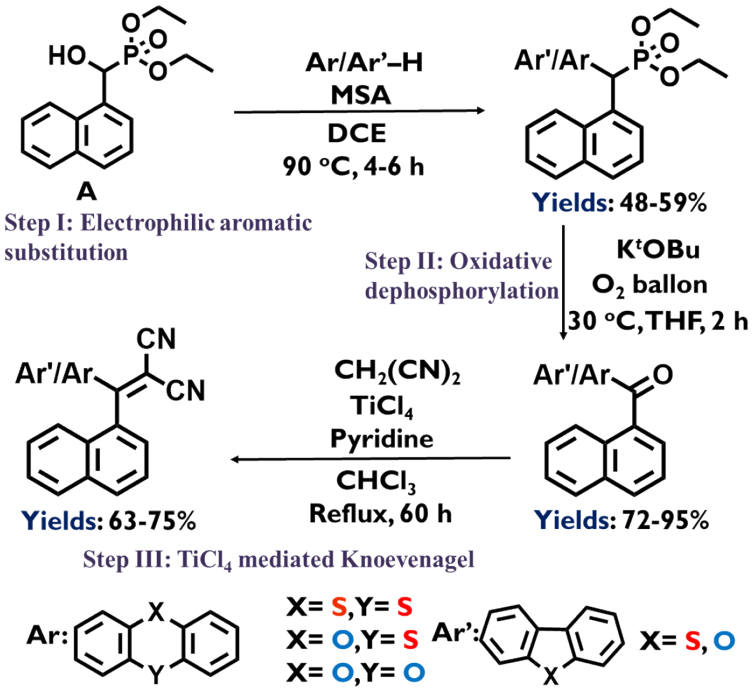

Fig. S1 Synthetic route of the compounds[1]

The synthetic procedure and stoichiometry were reported in detail elsewhere.[1]

Synthesis of 2-(naphthalen-1-yl(thianthren-2-yl)methylene)malononitrile (TANCN)

Yield ~75%, brightly orange-red fluorescent solids, **IR** (cm^{-1}): 3050, 2975, 2915, 2832, 2217, 1709, 1652, 1564, 1444, 1331, 1240, 1215, 1031; **mp**: 231°-233°C; **^{1}H NMR** (400 MHz, $CDCl_3$, 25°C) δ 8.07-8.05 (d, J = 8 Hz, 1H), 7.94-7.92 (d, J =.8 Hz, 1H), 7.61 (t, J = 8 Hz, 1H), 7.55-7.49 (m, 5H), 7.46-7.40 (m, 4H), 7.29-7.27 (m, 1H), 7.26-7.24 (m, 1H); **^{13}C NMR** (100 MHz, $CDCl_3$, 25°C) δ 172.7, 142.3, 136.9, 135.1, 133.9, 133.8, 133.1, 132.4, 131.6, 130.3, 129.0, 128.9, 128.7, 128.5, 128.3, 127.9, 126.9, 125.1, 124.7, 113.4, 113.0, 96.1, 84.9; **HRMS** (ESI) m/z: calcd. for $C_{26}H_{14}N_2S_2$ 418.0598, found 442.0515 $[M+Na]^+$.[1]

Synthesis of 2-(naphthalen-1-yl(phenoxathiin-3-yl)methylene)malononitrile (PONCN)

Yield ~71%, brightly orange-yellow fluorescent solids, **IR** (cm^{-1}): 3056, 2956, 2909, 2835, 2211, 1705, 1520, 1456, 1402, 1311, 1268, 1217, 1080, 1026; **mp**: 160°-162°C; **^{1}H NMR** (400 MHz, $CDCl_3$, 25°C) δ 8.00-7.98 (d, J = 8 Hz, 1H), 7.87-7.85 (d, J =.8 Hz, 1H), 7.55 (t, J = 8 Hz, 1H), 7.50-7.44 (m, 2H), 7.41-7.33 (m, 2H), 7.22-7.20 (m, 1H), 7.07-6.01 (m, 5H), 6.84-6.82 (m, 1H); **^{13}C NMR** (100 MHz, $CDCl_3$, 25°C) δ 172.5, 151.8, 150.8, 134.9, 133.9, 133.2, 132.2, 130.4, 128.9, 128.4, 127.8, 127.5, 127.1, 126.9, 126.7, 125.6, 125.1, 125.0, 124.7, 118.2, 117.9, 117.7, 113.5, 113.2, 96.1, 84.2; **HRMS** (ESI) m/z: calcd. for $C_{26}H_{14}N_2OS$ 402.0827, found 425.0626 $[M+Na]^+$.[1]

Synthesis of 2-(dibenzo[b,e][1,4]dioxin-2-yl(naphthalen-1-yl)methylene)malononitrile) (OXNCN)

Yield ~65%, brightly green fluorescent solids, **IR** (cm^{-1}): 3049, 2956, 2921, 2851, 2215, 1721, 1578, 1463, 1419, 1317, 1222, 1113, 1030; **mp**: 194°-196°; **^{1}H NMR** (400 MHz, $CDCl_3$, 25°C) δ 7.99-7.97 (d, J = 8 Hz, 1H), 7.87-7.85 (d, J =.8 Hz, 1H), 7.56-7.35 (m, 5H), 7.18-7.15 (m, 1H), 6.96-6.69 (m, 6H); **^{13}C NMR** (100 MHz, $CDCl_3$, 25°C) δ 172.2, 146.3, 142.5, 141.3, 133.9, 133.3, 132.1, 131.2, 130.4, 128.9, 128.3, 127.7, 126.9, 126.5, 124.9, 124.4, 117.8, 117.1, 116.6, 113.8, 113.3, 96.1, 83.3; **HRMS** (ESI) m/z: calcd. for $C_{26}H_{14}N_2O_2$ 386.1055, found 409.0925 $[M+Na]^+$.[1]

Synthesis of 2-(dibenzo[b,d]thiophen-3-yl(naphthalen-1-yl)methylene)malononitrile (DBTNCN)

Yield ~74%, brightly cyan-green fluorescent solids, **IR** (cm^{-1}): 3052, 2942, 2898, 2826, 2213, 1702, 1590, 1524, 1411, 1325, 1238, 1152, 1065; **mp**: 217°-219°C; **^{1}H NMR** (400 MHz,

$CDCl_3$, 25°C) δ 8.46 (s, 1H), 8.11-8.07 (m, 2H), 7.95 (d, J = 8 Hz, 1H), 7.88-7.85 (m, 2H), 7.67-7.63 (m, 2H), 7.57-7.45 (m, 5H), 7.41-7.37 (m, 1H); **^{13}C NMR** (100 MHz, $CDCl_3$, 25°C) δ 174.2, 144.9, 139.8, 136.1, 134.6, 133.9, 133.7, 132.2, 131.9, 130.6, 128.9, 128.6, 127.9, 127.7, 127.4, 126.9, 125.2, 124.9, 123.5, 123.0, 122.7, 122.1, 114.1, 113.5, 96.1, 83.9; **HRMS** (ESI) m/z: calcd. for $C_{26}H_{14}N_2S$ 386.0878, found 410.0793 $[M+Na]^+$.[1]

Synthesis of 2-(dibenzo[b,d]thiophen-3-yl(naphthalen-1-yl)methylene)malononitrile (DBFNCN)

Yield ~63%, brightly cyan fluorescent solids, **IR** (cm^{-1}): 3059, 2954, 2929, 2851, 2220, 1747, 1579, 1534, 1430, 1321, 1250, 1188, 1127, 1025; **mp**: 169°-171°C; **^{1}H NMR** (400 MHz, $CDCl_3$, 25°C) δ 8.23-8.06 (m, 2H), 8.03-7.90 (m, 2H), 7.73-7.55 (m, 5H), 7.54-7.43 (m, 3H), 7.41-7.34 (m, 2H); **^{13}C NMR** (100 MHz, $CDCl_3$, 25°C) δ 166.5, 157.6, 155.7, 149.6, 133.9, 132.3, 130.6, 129.3, 129.2, 128.9, 128.6, 127.7, 126.8, 125.1, 124.9, 124.4, 123.6, 123.5, 122.9, 122.7, 121.6, 121.3, 121.2, 113.9, 113.3, 112.1; **HRMS** (ESI) m/z: calcd. for $C_{26}H_{14}N_2O$ 370.1106, found 393.0999 $[M+Na]^+$.[1]

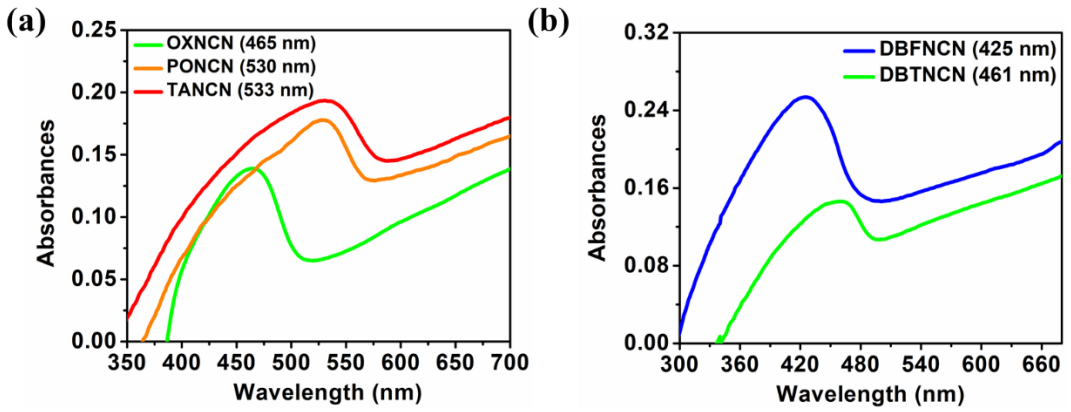

Fig. S2. Absorbances in solid-state for compounds of (a) six-membered ring series, (b) five-membered ring series

Table S1 Crystal parameters for **TANCN**, **PONCN**, and **DBTNCN**

Topic	**TANCN**	**PONCN**	**DBTNCN**
Emp. Formula	$C_{26}H_{14}N_2S_2$	$C_{26}H_{14}N_2OS$	$C_{26}H_{14}N_2S$
Formula weight	418.5320	402.4710	386.4720
Crystal system	Monoclinic	Monoclinic	Monoclinic

Space group	P 1 21/n 1	P 1 21/n 1	P 1 21/c 1
a/Å	11.9694 (1)	11.6522 (2)	10.2590 (2)
b/Å	10.1347 (1)	10.1365 (2)	23.9746 (5)
c/Å	16.2523 (2)	16.2509 (3)	7.6877 (2)
/degree	90	90	90
/degree	96.470 (1)	98.031 (2)	94.982 (2)
/degree	90	90	90
V/ Å^3	1958.95 (4)	1900.61 (6)	1883.69 (7)
Z	4	8	4
$D_{calc/g\ cm-3]}$	1.419	1.406	1.363
/mm^{-1}	2.570	1.677	1.627
F(000)	809.0	832.0	803.5
Data/restraints/parameters	4135/0/272	4029/0/272	3976/0/263
S	1.053	1.078	1.018
+R1 [I>2(I)]	0.0342 (3946)	0.0525 (3761)	0.0366 (3607)
wR2 [all data]	0.0916 (4135)	0.1340 (4029)	0.0998 (3976)
Max./min. residual electron dens. [eÅ^{-3}]	0.324/-0.321	0.841/-0.501	0.2754/-0.4077
CCDC No.	2356941	2356952	2356943

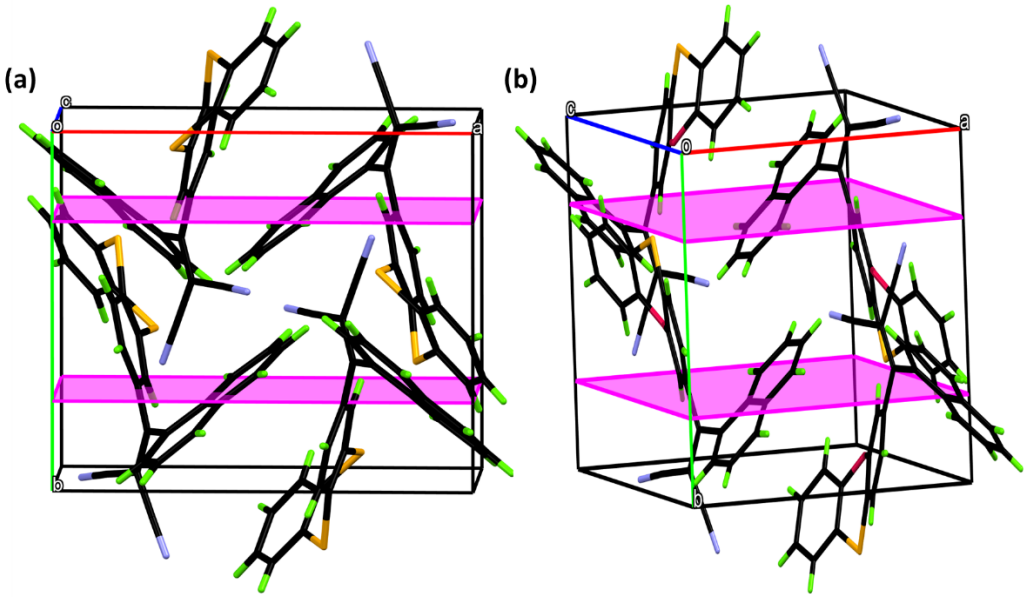

Fig. S3. Glide planes from 'b' axis view for (a) **TANCN** (b) **PONCN**

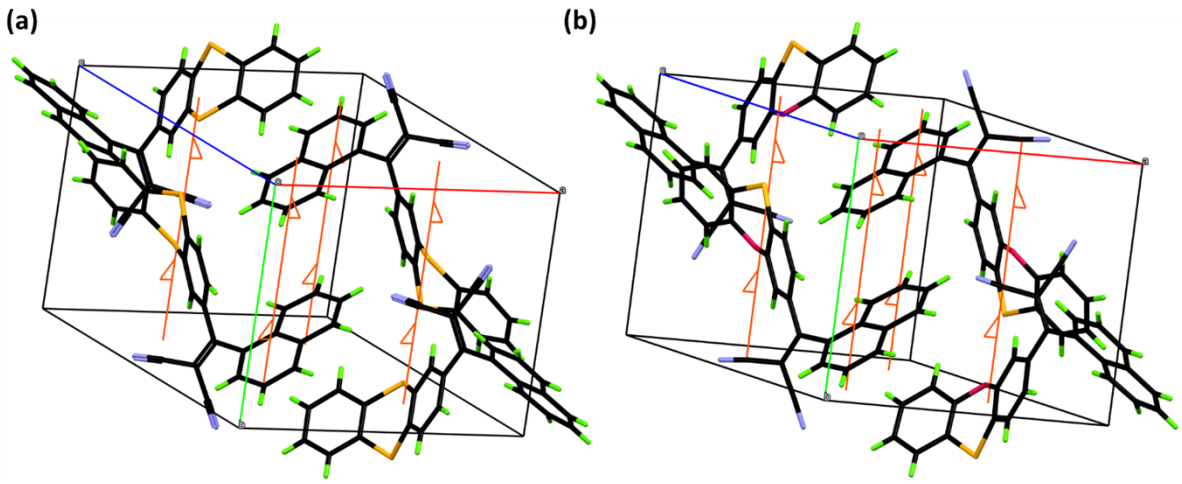

Fig. S4. Two-fold Screw-axes from 'b' axis view for (a) **TANCN** (b) **PONCN**

Table S2 Non-covalent interactions in **TANCN** and **PONCN**

Molecules	**C…C (Å)**	**C…H/H…C (Å)**	**N…H/H…N (Å)**	**H…H (Å)**	**O…H (Å)**	**S…S (Å)**	**S…H (Å)**
PONCN	3.153, 3.266, 2.924, 2.957, 3.327, 3.335, 3.315, 3.390	2.653, 2.731, 2.767, 2.703, 2.679, 2.490, 2.614, 2.847, 2.824,	2.746, 2.709, 2.542	2.372	2.682	absent	absent
TANCN	2.916, 3.303, 3.116, 2.975, 3.350, 3.294, 3.272, 3.273	2.739, 2.722, 2.739, 2.717, 2.507, 2.601, 2.631, 2.889	2.738, 2.748, 2.725	absent	absent	3.575	2.906

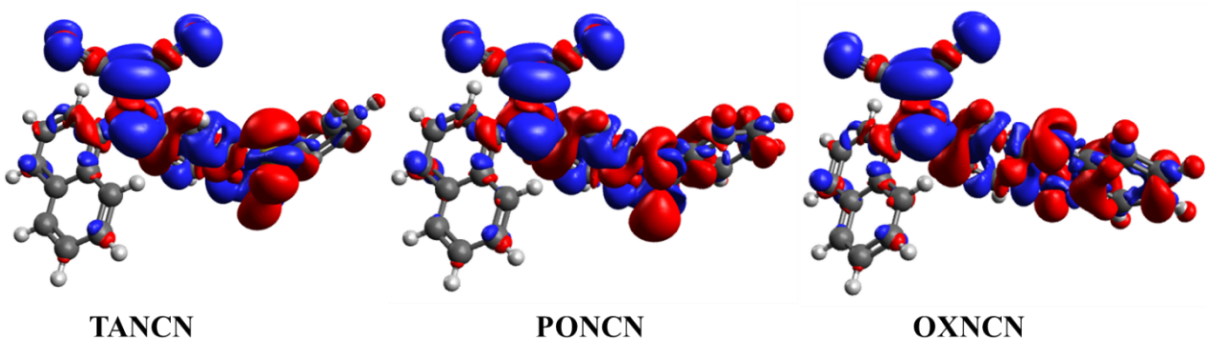

Fig. S5. Electron density map, the blue and red color denotes the high electron density in the ground and excited states, respectively. The isovalue is 0.001 a.u. (gas phase)

Table S3 Dipolemoments (in Debye) in the X, Y, and Z axes

1) **exp_873_TANCN**

0.2957 1.1181 -0.4619 (1st molecule)
0.2957 -1.1181 -0.4619 (2nd molecule)
0.2957 1.1181 -0.4619 (3rd molecule)
Angle between 1 and 2: 127.74 degrees
Angle between 2 and 3: 127.74 degrees
Angle between 1 and 3: 0 degrees

2) **exp_1385_PONCN**

0.4860 -1.5071 -0.7792 (1st molecule)
0.4860 1.5071 -0.7792 (2nd molecule)

0.4860 -1.5071 -0.7792 (3rd molecule)
Angle between 1 and 2: 117.28 degrees
Angle between 2 and 3: 117.28 degrees
Angle between 1 and 3: 0 degrees

Table S4 Calculated inter-molecular potentials for **PONCN**

mol1 mol2 distance energy (kJ/mol)
0 1 6.24483 -59.6034
2 3 9.06743 -40.5849
4 5 9.06743 -40.5849
2 4 7.25153 -40.1323
2 5 10.7775 -36.3206
0 6 8.59504 -27.5489

Hydrogen normalisation: Off

Cluster Energy:
PE = -208.39 kJ/mol 40 interactions
PE = -211.72 kJ/mol 120 interactions
PE = -212.04 kJ/mol 160 interactions
PE = -212.14 kJ/mol 180 interactions
PE = -212.18 kJ/mol 190 interactions
PE = -212.20 kJ/mol 200 interactions

Total packing energy = -212.2 kJ/mol

Potential = A*exp(-Br) - Cr(-6)

Unified (UNI) pair-potential parameters:
atom1 code1 atom2 code2 A B C
S001 9 S001 9 1087673.0 3.52 10757.1
S001 9 O002 16 460903.9 3.63 3789.1
S001 9 N003 23 630306.9 3.59 5576.8
S001 9 C005 3 529108.6 3.41 6292.7
S001 9 H00D 1 268571.0 4.03 1167.3
O002 16 O002 16 195309.1 3.74 1335.0
O002 16 N003 23 268571.0 3.86 1523.0
O002 16 C005 3 393086.8 3.74 2682.0
O002 16 H00D 1 295432.3 4.82 439.3
N003 23 N003 23 365263.0 3.65 2891.0
N003 23 C005 3 491494.0 3.86 2791.0
N003 23 H00D 1 228279.0 4.52 502.1
C005 3 C005 3 226145.2 3.47 2418.0
C005 3 H00D 1 120792.1 4.10 472.8
H00D 1 H00D 1 24158.0 4.01 109.2

Table S5 Calculated inter-molecular potentials for **TANCN**

mol1 mol2 distance energy (kJ/mol)
0 1 6.38397 -56.0314
0 2 9.05056 -43.7961
3 4 10.7286 -41.6731
5 4 7.6038 -34.4395
0 6 8.4522 -29.2629

Hydrogen normalisation: Off

Cluster Energy:
PE = -215.07 kJ/mol 40 interactions
PE = -218.47 kJ/mol 120 interactions
PE = -218.79 kJ/mol 160 interactions
PE = -218.90 kJ/mol 180 interactions
PE = -218.93 kJ/mol 190 interactions
PE = -218.96 kJ/mol 200 interactions

Total packing energy = -219.0 kJ/mol
Potential = A*exp(-Br) - Cr(-6)

Unified (UNI) pair-potential parameters:
atom1 code1 atom2 code2 A B C
S01 9 S01 9 1087673.0 3.52 10757.1
S01 9 N1 23 630306.9 3.59 5576.8
S01 9 C005 3 529108.6 3.41 6292.7
S01 9 H00B 1 268571.0 4.03 1167.3
N1 23 N1 23 365263.0 3.65 2891.0
N1 23 C005 3 491494.0 3.86 2791.0
N1 23 H00B 1 228279.0 4.52 502.1
C005 3 C005 3 226145.2 3.47 2418.0
C005 3 H00B 1 120792.1 4.10 472.8
H00B 1 H00B 1 24158.0 4.01 109.2

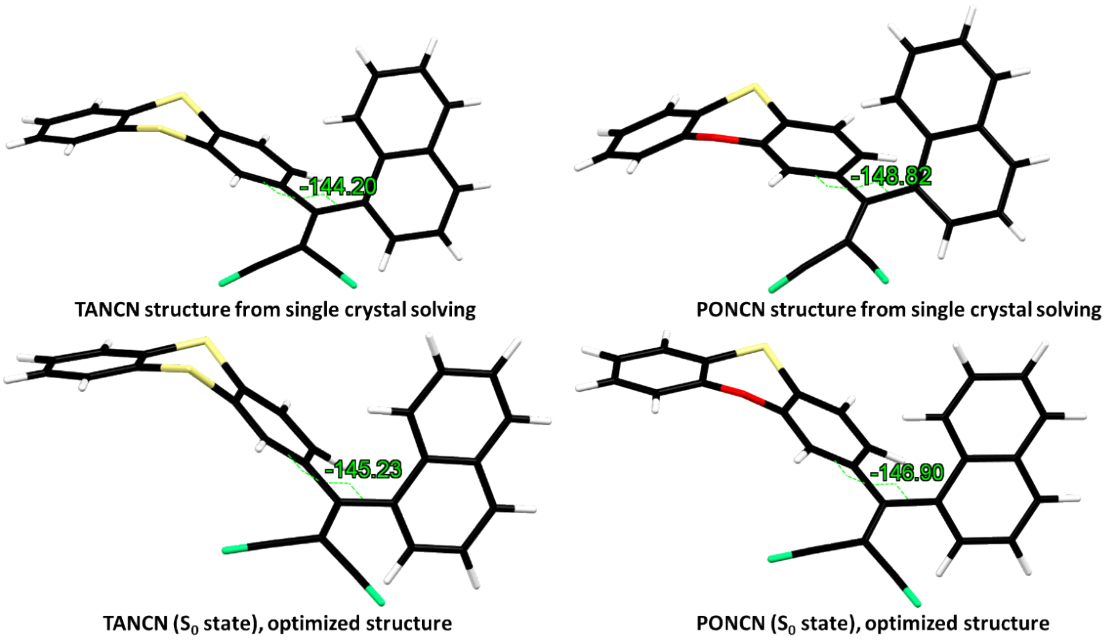

Fig. S6. Comparison between single-crystal solved structures and TD-DFT optimized structures (gas phase) of **TANCN** and **PONCN**.

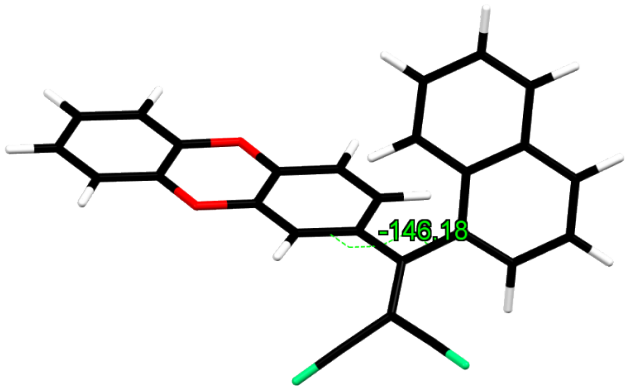

Fig. S7. TD-DFT optimized structure (S_0 state, gas phase) of **OXNCN**.

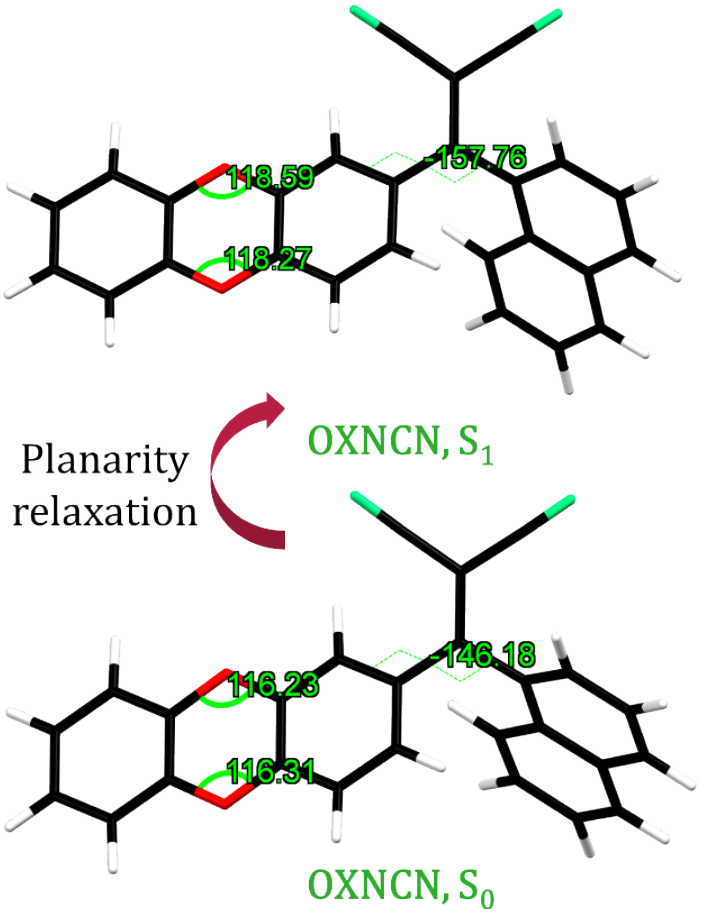

Fig. S8. Comparison of the ground state (S_0) vs excited state (S_1) planarity in respective molecules in the gas phase

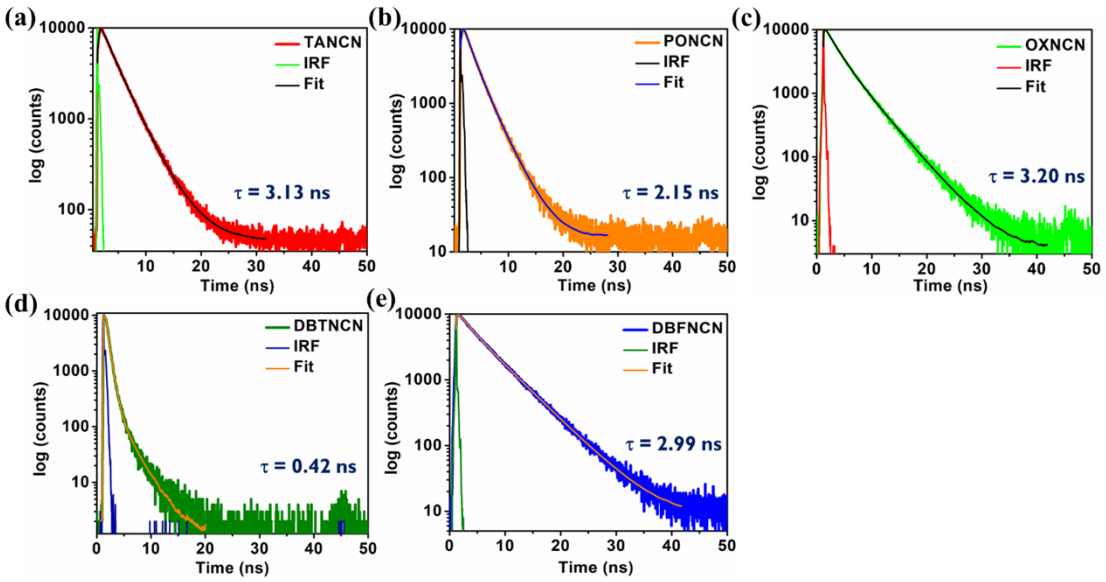

Fig. S9. Lifetime decay profiles for **TANCN**, **PONCN**, **OXNCN**, **DBTNCN**, and **DBFNCN** solids;

Table S6 TD-DFT calculated bond angles (all the angles are in degree unit) at heteroatomic centres and torsion angle ($\theta_{h\text{-}n}$) between heterocycles and flanking tilted naphthalene (using B3LYP/6-31g(d) level of theory)

Compounds	S_0 ∠C-S-C	S_1 ∠C-S-C	S_0 ∠C-O-C	S_1 ∠C-O-C	$\theta_{h\text{-}n}$ (S_0)	$\theta_{h\text{-}n}$ (S_1)
OXNCN	-	-	116.31 116.23	118.27 118.59	-146.18	-157.76
PONCN	117.89	124.57	97.86	102.27	-146.90	-158.09
TANCN	100.55 100.18	107.04 107.39	-	-	-145.23	-159.51
DBFNCN	-	-	106.05	105.96	-147.39	-153.11
DBTNCN	91.01	90.81	-	-	148.34	173.08

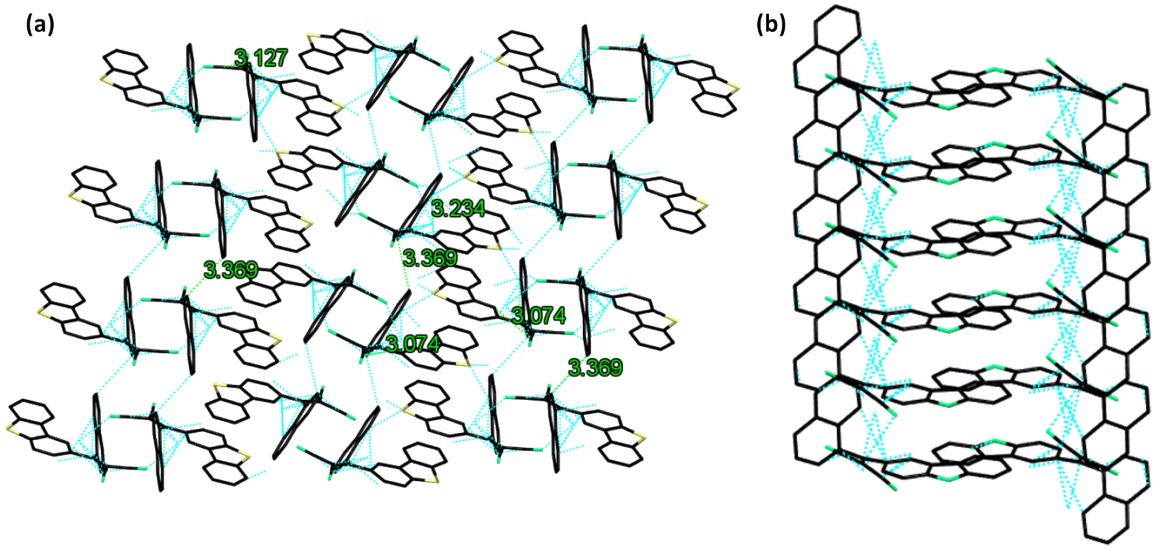

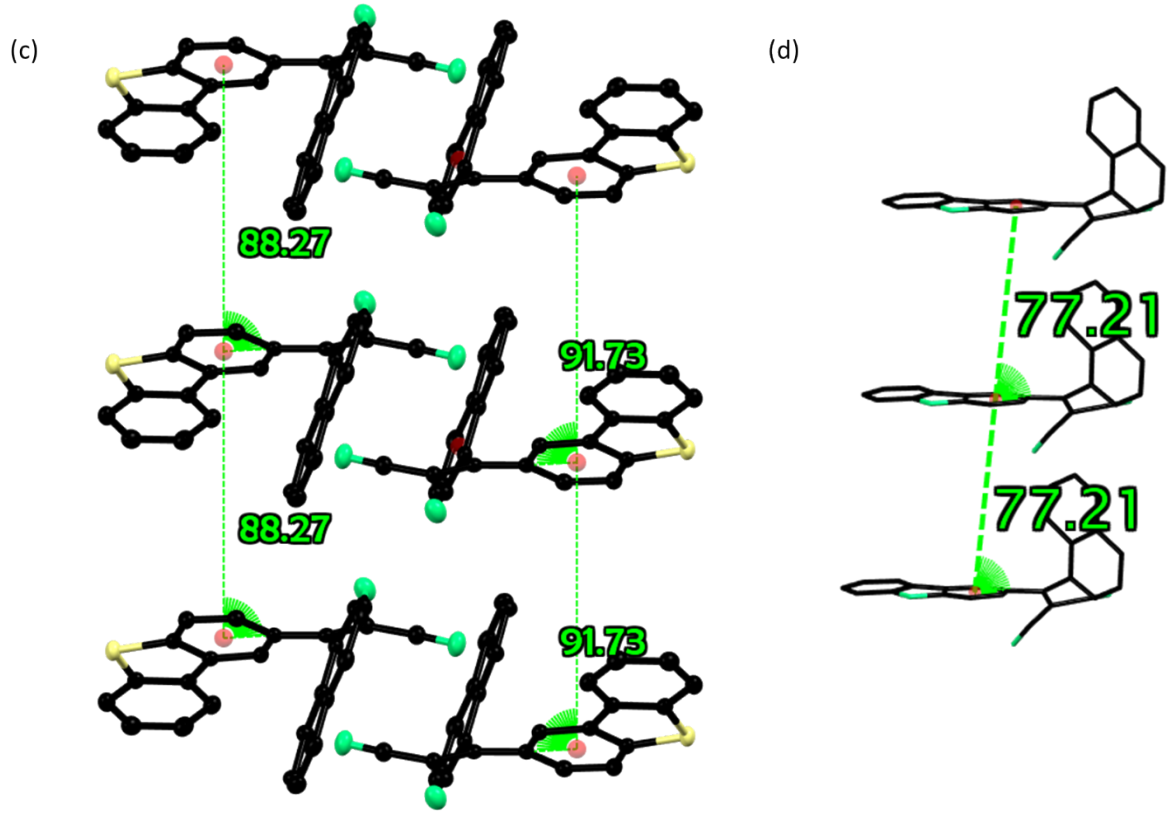

Fig. S10. Crystal-packing with non-covalent interactions for (a) **DBTNCN** (solved) and (b) **DBFNCN** (attempted, could not be solved with R<10 and wR2<30), slip-stack orientation for (c) **DBTNCN** and (d) **DBFNCN** (probable)

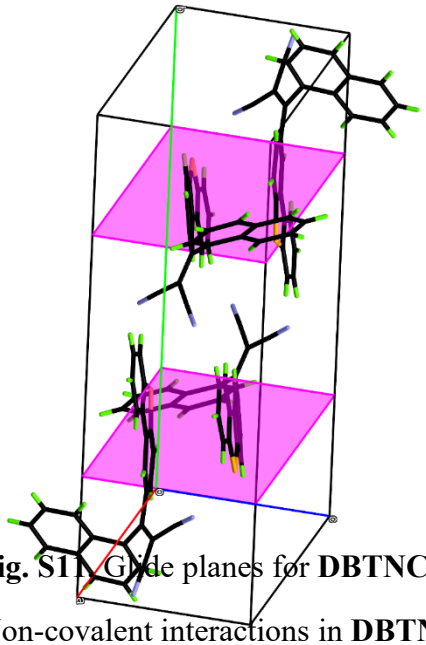

Fig. S11. Glide planes for **DBTNCN**

Table S7 Non-covalent interactions in **DBTNCN** crystal

Compound	C...C (Å)	C...H/H...C (Å)	N...H/H...N (Å)	S...H (Å)
DBTNCN	3.234, 3.074,	2.759, 2.631,	2.650, 2.644,	2.972, 2.961

	3.127, 3.369,	2.647, 2.838, 2.625, 2.831, 2.898		

Table S8 Summary of the results of solid-state time-resolved spectroscopic studies; The k_r and k_{nr} are calculated only when the lifetime is determined as >1 ns

Compounds	τ_1 (ns)	τ_2 (ns)	τ_3 (ns)	α_1	α_2	α_3	χ^2	τ (ns)	Φ_f (%)	k_r (s^{-1})×10^6	k_{nr} (s^{-1})×10^6
TANCN	2.735	4.044	-	0.698	0.302	-	0.977	3.13	9.60	30.67	288.82
PONCN	1.546	2.829	-	0.532	0.468	-	1.16	2.15	3.00	13.95	451.16
OXNCN	2.075	4.385	-	0.514	0.486	-	1.104	3.20	10.22	31.94	280.56
DBTNCN	0.183	0.611	2.354	0.603	0.448	0.017	1.17	<1 ns	6.79	-	-
DBFNCN	2.163	5.235	-	0.728	0.272	-	1.087	2.99	8.36	27.96	306.49

Table S9 ΔE_{ST} values of compounds [M06-2X/6-31G(d) level of theory with a time-dependent density functional theory (TD-DFT) approach]

Molecules	Solvents	S_1 (eV)	T_1 (eV)	ΔE_{ST} (eV)
DBTNCN	Hexane	3.699	2.879	0.820
	DCM	3.629	2.879	0.750
	GAS	3.793	2.885	0.909
PONCN	Hexane	3.528	2.817	0.710
	DCM	3.502	2.816	0.685
	GAS	3.595	2.825	0.770
TANCN	Hexane	3.644	2.878	0.767
	DCM	3.570	2.877	0.693
	GAS	3.716	2.883	0.833
OXNCN	Hexane	3.503	2.772	0.732
	DCM	3.448	2.754	0.694
	GAS	3.592	2.791	0.801
DBFNCN	Hexane	3.732	2.918	0.815
	DCM	3.660	2.916	0.745
	GAS	3.831	2.924	0.907

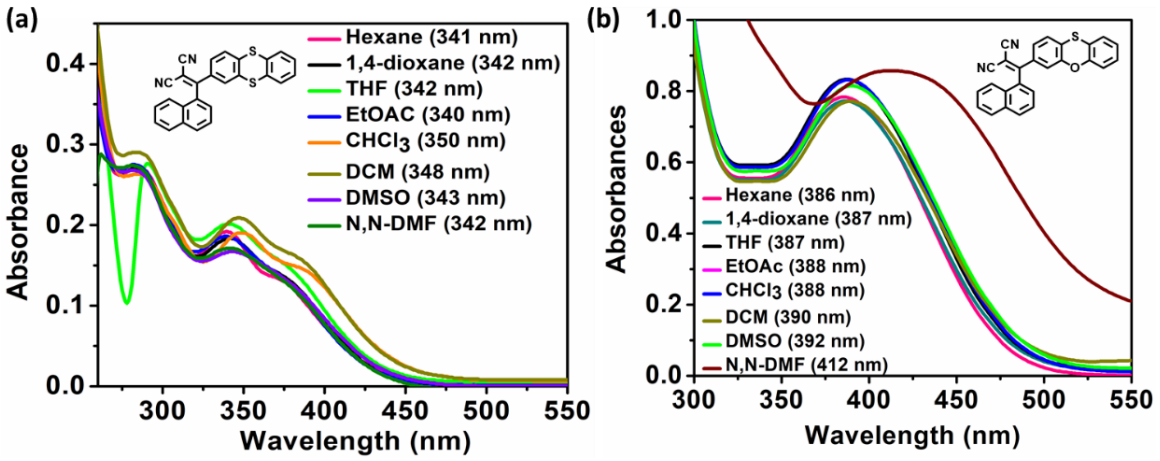

Fig. S12. Solution-state absorbances in different solvents with different polarity for (a) **TANCN** (b) **PONCN**

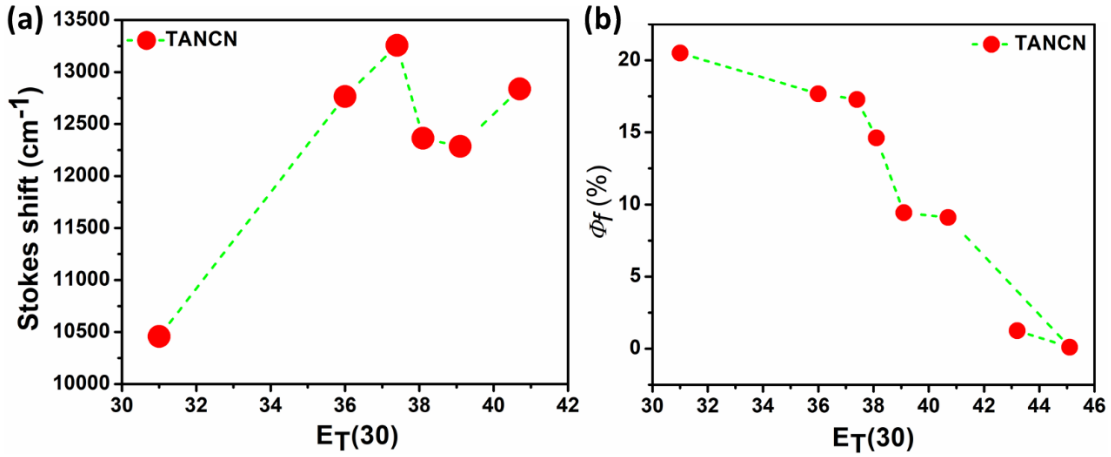

Fig. S13. Plots for solvatochromism of **TANCN** (a) Stokes Shift vs $E_T(30)$ (b) Φ_f(%) vs $E_T(30)$

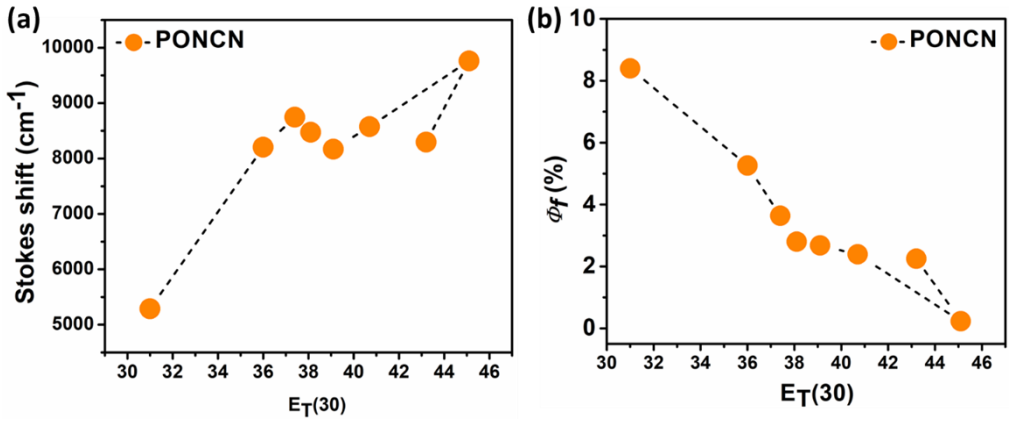

Fig. S14. Plots for solvatochromism of **PONCN** (a) Stokes Shift vs $E_T(30)$ (b) Φ_f(%) vs $E_T(30)$

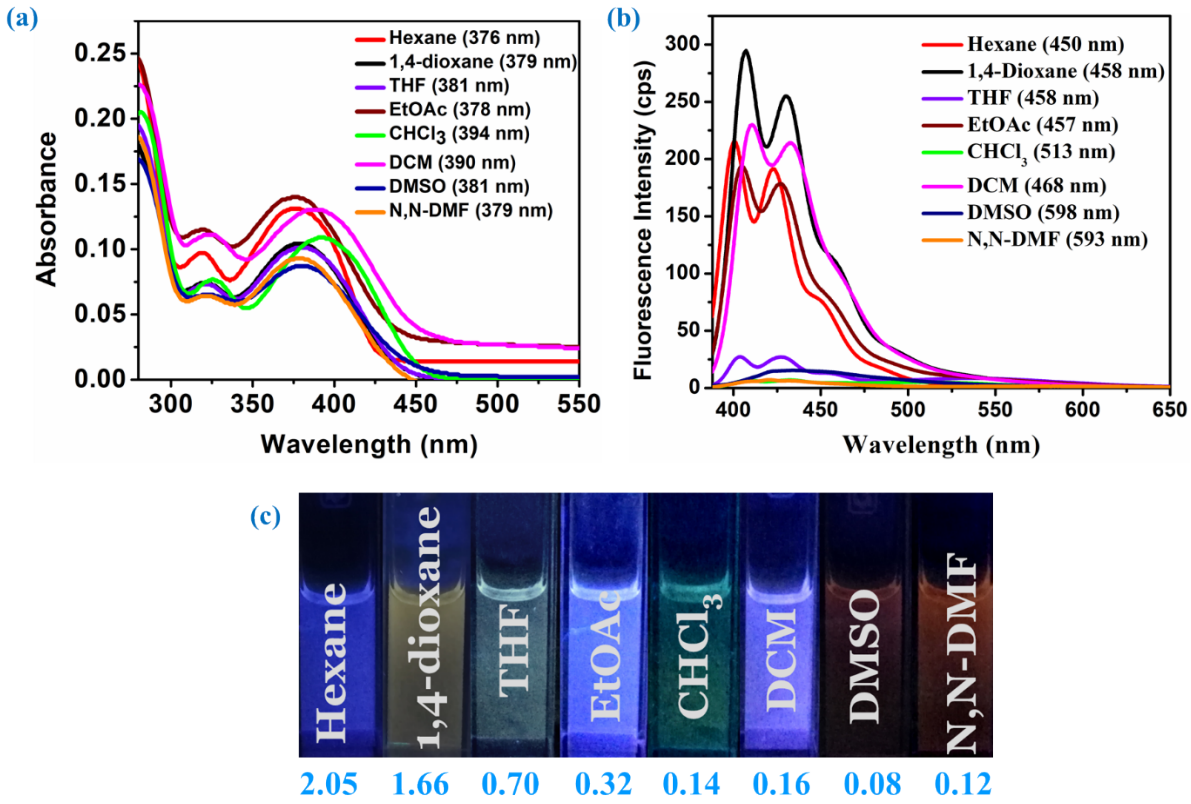

Fig. S15. Solid and solution state emission for **OXNCN** (10^{-5} M) (a) absorbances (b) emissions (c) images captured under UV-365 nm bulb; the image of green solid-state emission is kept inset, the Φ_f (%) in respective solvents are written in red below the picture[1]

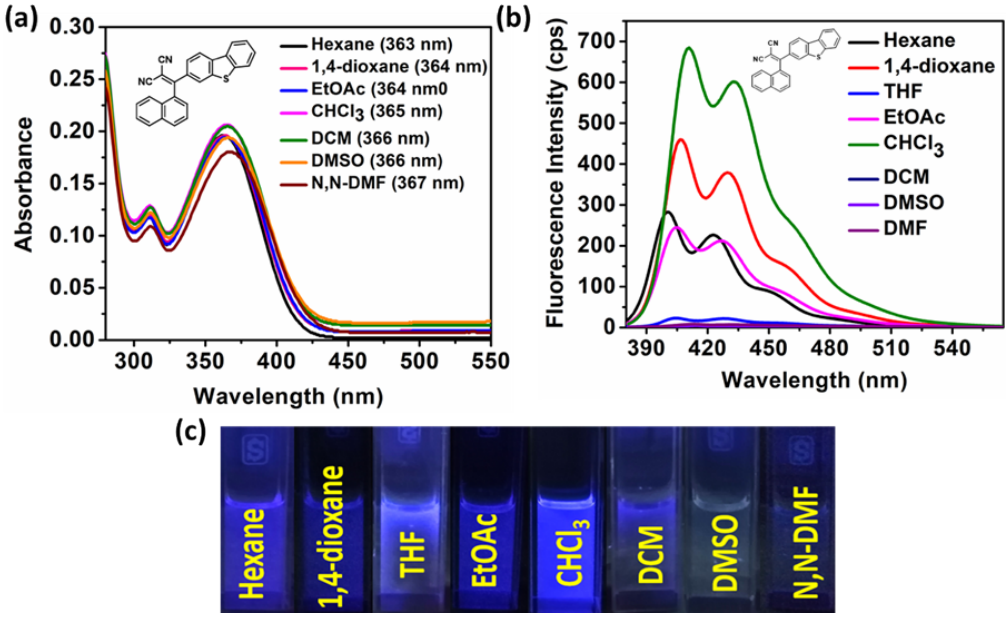

Fig. S16. Solution state photophysical profile for **DBTNCN** (a) absorbances (b) emissions (c) picture captured under UV-365 nm bulb for respective solvents

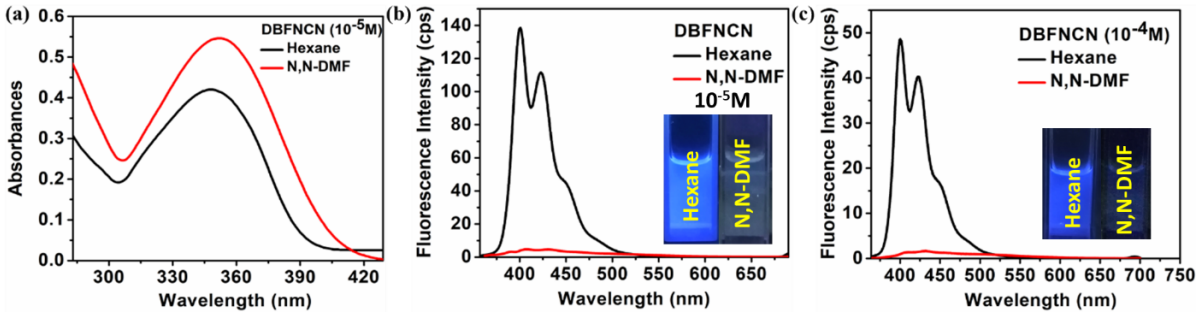

Fig. S17. Solution state photophysical profile for **DBFNCN** (a) absorbances (b) emissions at 10^{-5} M probe concentration (c) emissions at 10^{-4} M probe concentration, inset pictures were captured under UV-365 nm bulb for respective solvents; excited at respective absorbances that remained the same for both the concentrations [$\lambda_{abs.max.}$(hexane)= 349 nm, $\lambda_{abs.max.}$(N,N-DMF) = 352 nm]

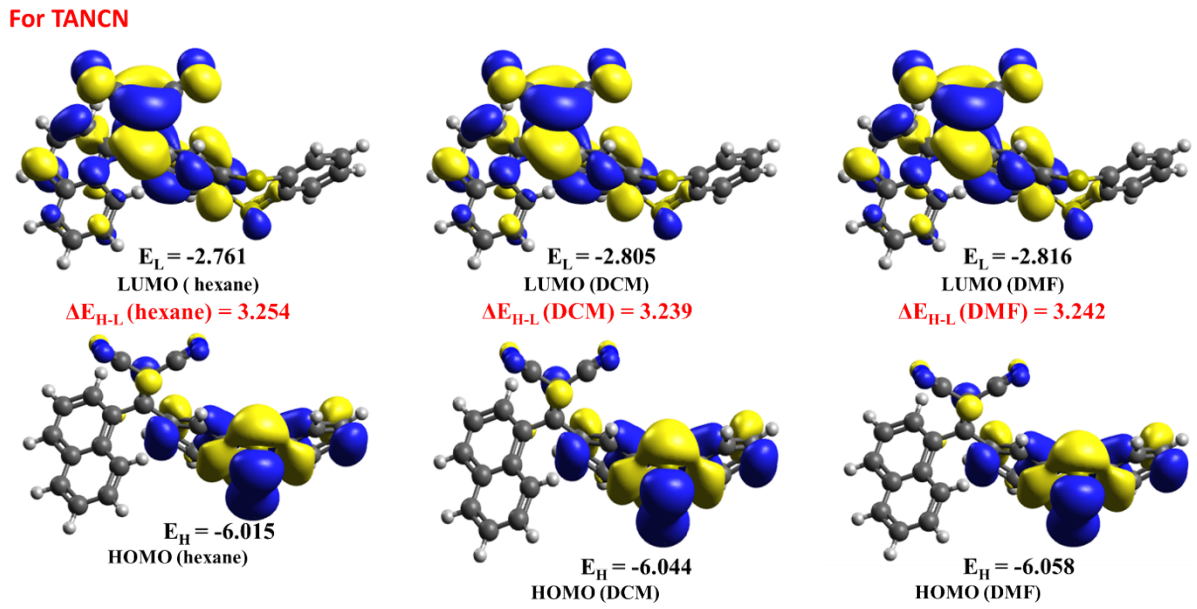

Fig. S18. For **TANCN**, HOMO-LUMO distribution in certain solvents

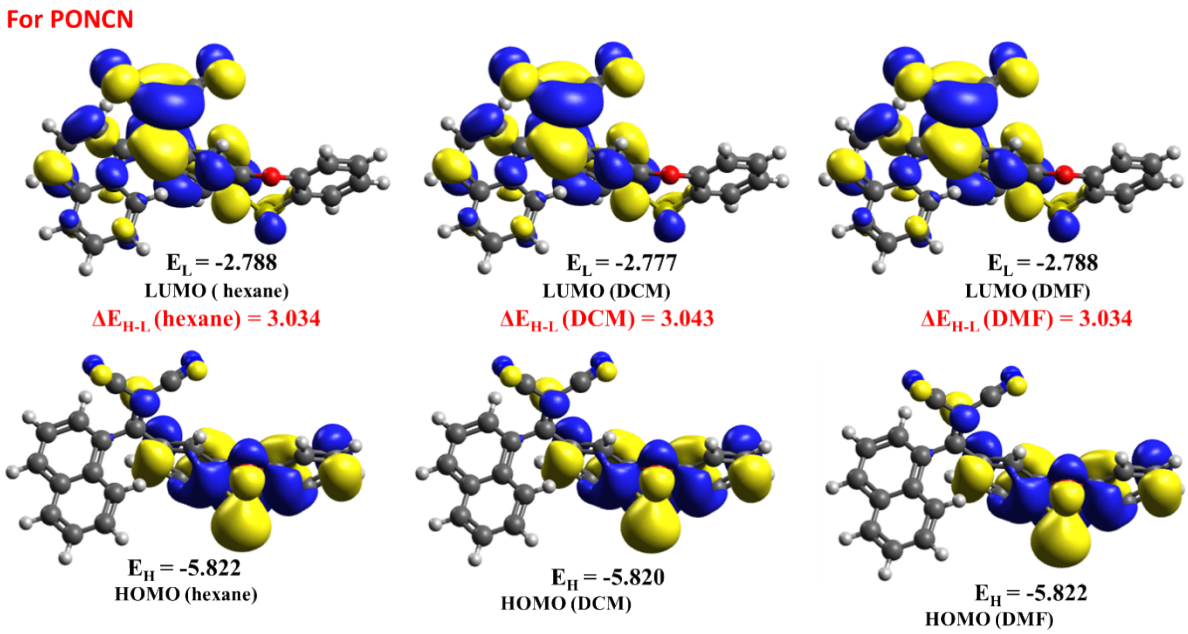

Fig. S19. For **PONCN**, HOMO-LUMO distribution in certain solvents

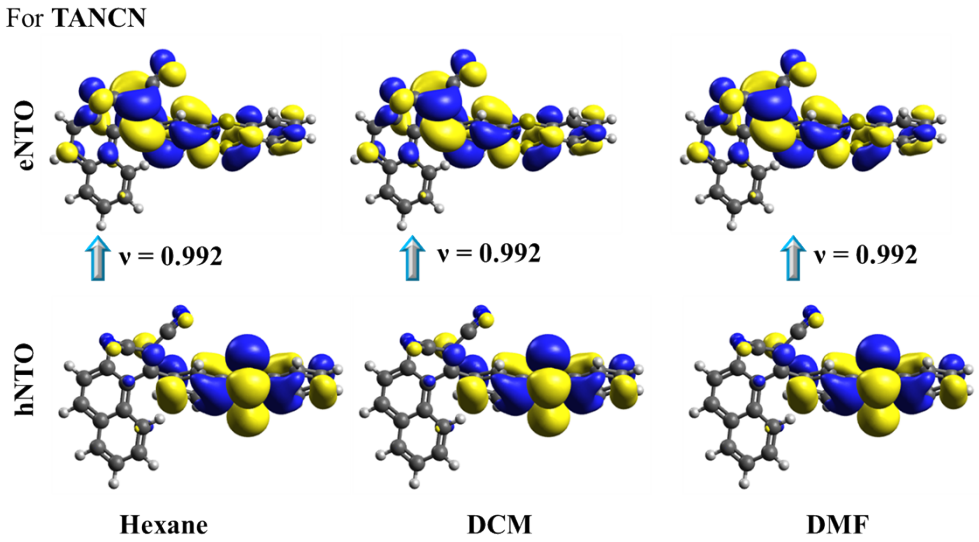

Fig. S20. For **TANCN**, NTOs in respective solvents

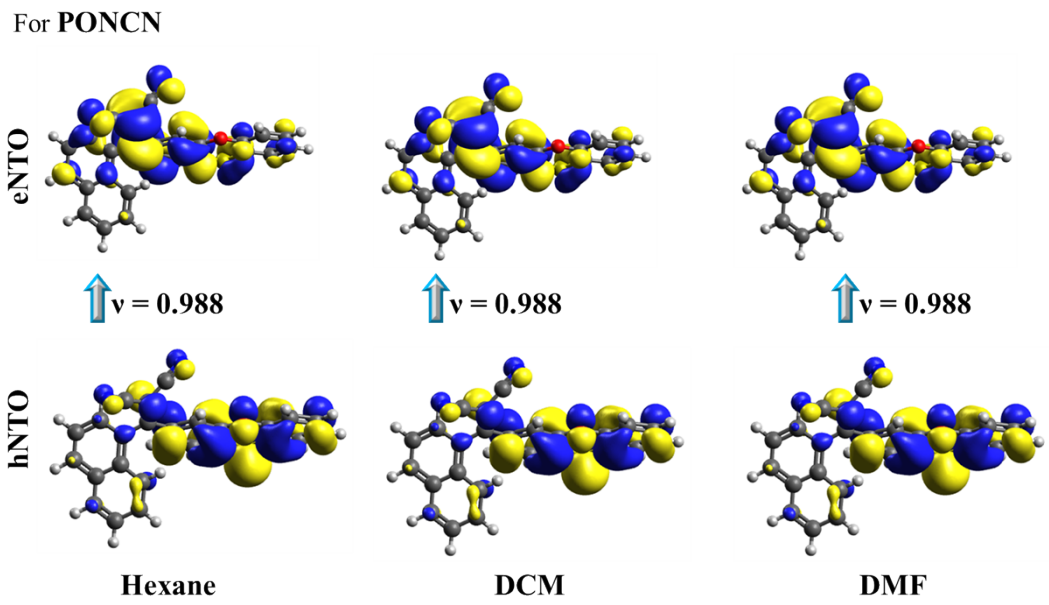

Fig. S21. For **PONCN**, NTOs in respective solvent

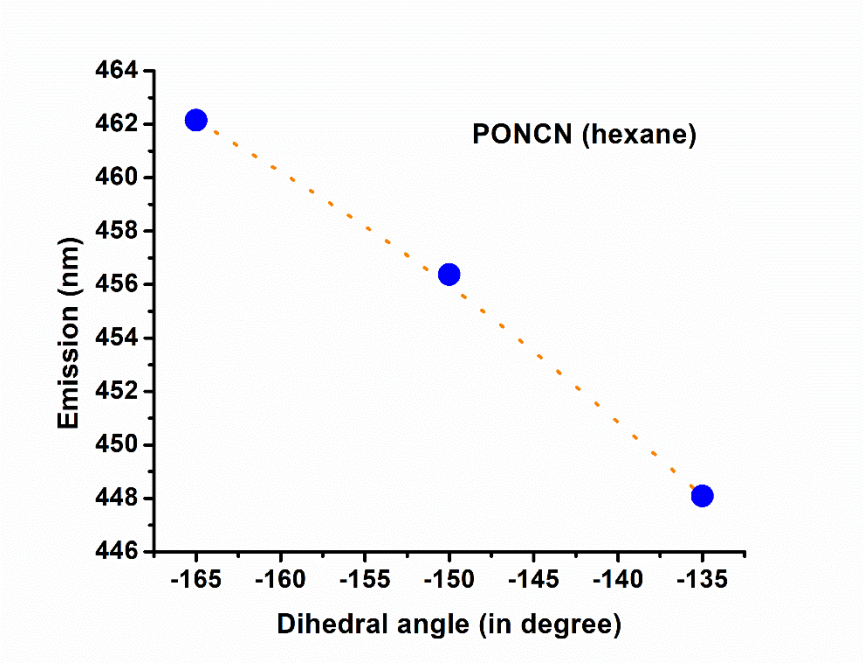

Fig. S22. Dihedral angle ($\theta_{h\text{-}n}$) vs emission scan in hexane for **PONCN**

Table S10 Solvent-wise orbital contribution

Compounds	Solvent	Orbital contribution	CT/LE
TANCN	Hexane	H-1→L (74%)	LE+CT
	DCM	H-1→L (92%)	LE+CT
PONCN	Hexane	H→L (89%)	LE+CT
	DCM	H→L (87%)	LE+CT

Table S11 DFT and TDDFT calculated parameters for **OXNCN**

Solvents	ΔE_{H-L} (eV)	Orbital contribution
Hexane	3.11	H→L (90%)
DCM	3.04	H→L (89%)
N,N-DMF	3.03	H→L (89%)

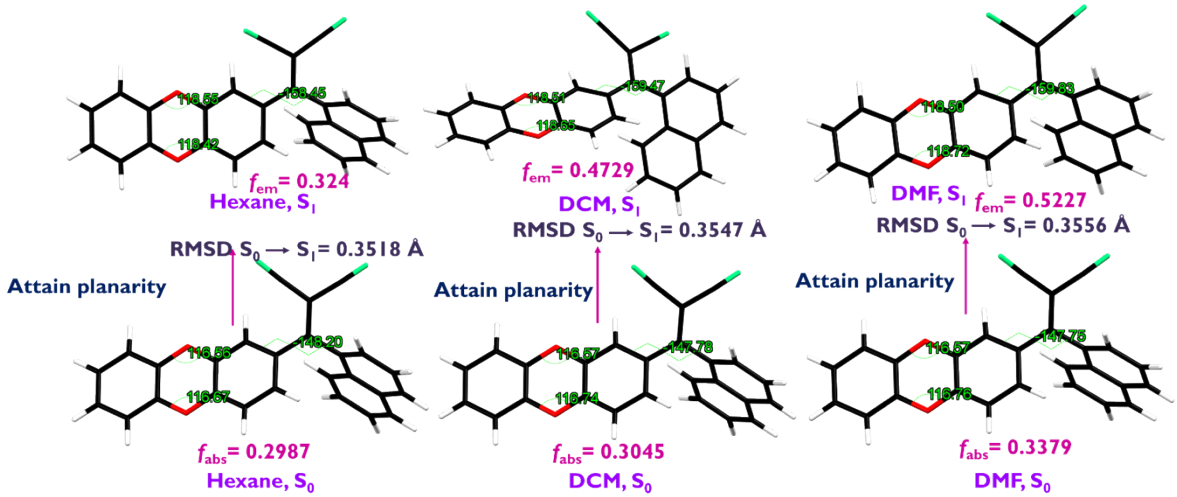

Fig. S23. DFT/TD-DFT optimized structures of **OXNCN** at different solvents with other quantum chemical descriptors at the S_0 and S_1 state

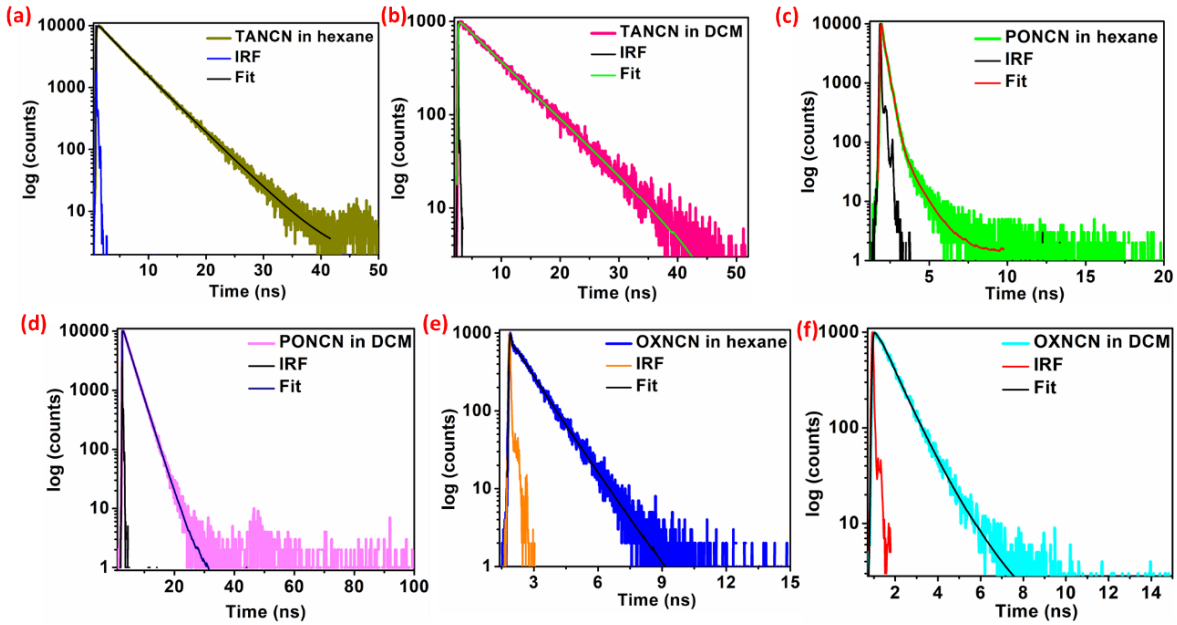

Fig. S24. Time-correlated single photon counting (TCSPC) decay curves for **TANCN**, **PONCN**, and **OXNCN** in hexane and DCM

Table S12 Summary of TCSPC results for emissions in solvents, radiative rate constant (k_r)= Φ_f/τ; non-radiative rate constant (k_{nr}) = (1- Φ_f)/τ_f; The k_r and k_{nr} are calculated only when the lifetime is determined as >1 ns

Compounds (solvents)	τ_1 (ns)	τ_2 (ns)	τ_3 (ns)	α_1	α_2	α_3	χ^2	τ (ns)	Φ_f (%)	k_r(s^{-1})×10^6	k_{nr}(s^{-1})×10^6
TANCN (hexane)	2.344	4.819	-	0.1196	0.8799	-	1.107	4.52	20.50	45.3	175.9
TANCN (DCM)	5.264	7.444	-	0.1619	0.8381	-	1.121	7.09	9.10	12.8	128.2
PONCN (hexane)	0.076	0.224	0.9184	0.3844	0.6036	0.012	0.976	<1 ns	8.40		
PONCN (DCM)	2.09	2.939	-	0.155	0.855	-	1.19	2.84	2.39	8.415	343.7
OXNCN (hexane)	0.02	0.534	1.085	0.9219	0.0574	0.0207	0.96	<1 ns	2.05		
OXNCN (DCM)	0.762	1.323	-	0.8033	0.1972	-	1.022	<1 ns	0.08		

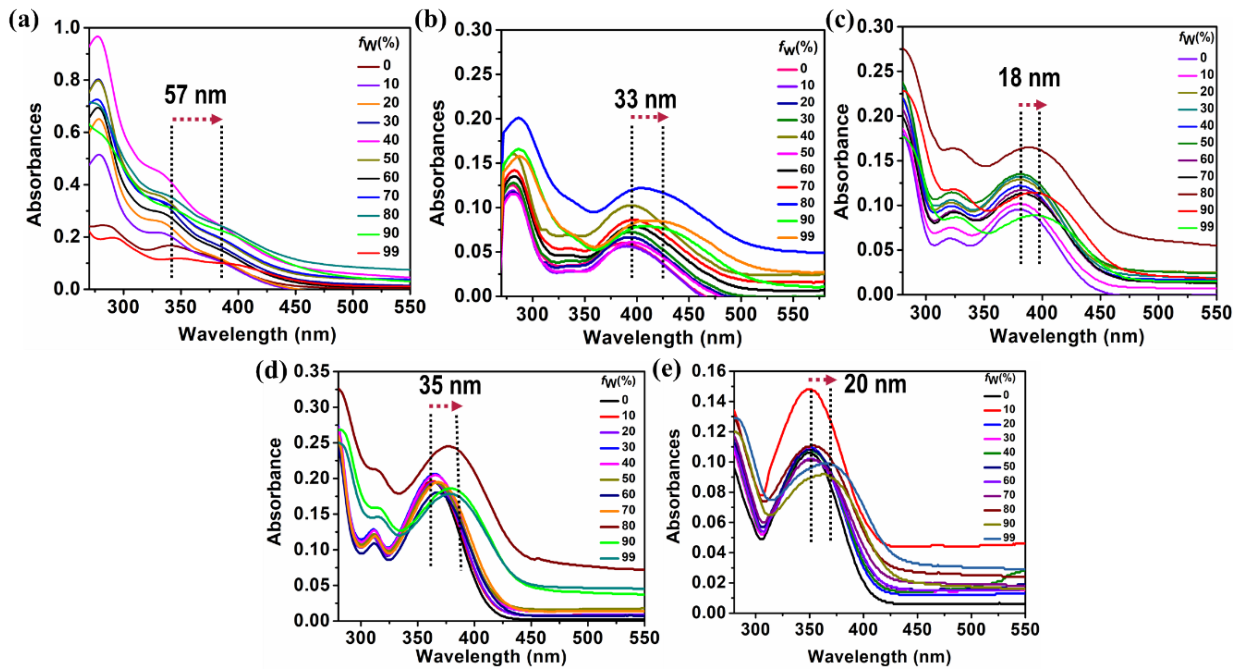

Fig. S25. Absorbance shifts on aggregation for the synthesized compounds: (a) **TANCN**, (b) **PONCN**, (c) **OXNCN**, (d) **DBTNCN**, (e) **DBFNCN**

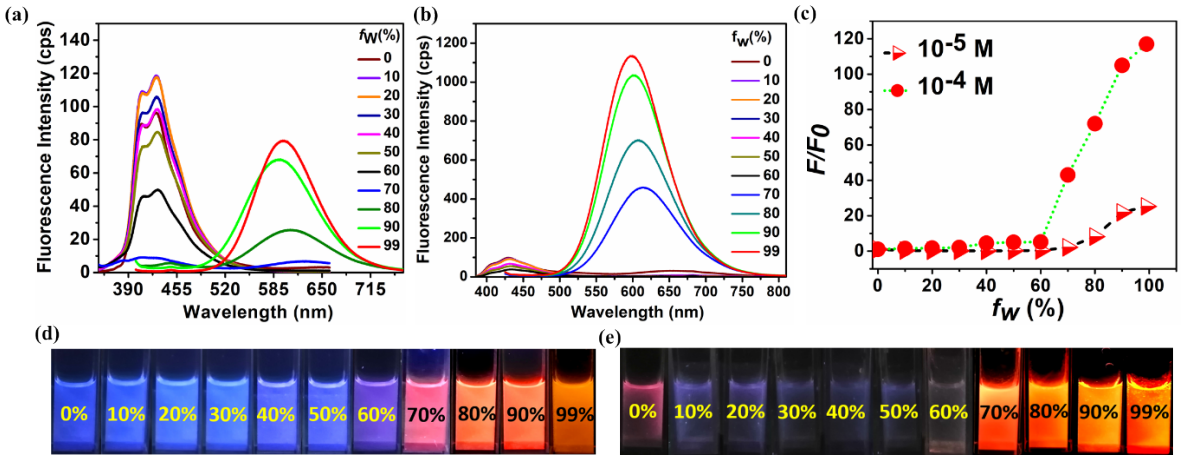

Fig. S26. AIE-property of **TANCN**, emissions with probe concentrations of (a) 10^{-5} M (b) 10^{-4} M (c) F/F_0 vs f_w (%) plot [f_w (%) is the added water fraction, F_0 is the emission intensity at f_w (%) = 0, and F is the emission intensity at the aggregate forming f_w (%)]; images captured under UV-365 nm bulb for **TANCN** (d) 10^{-5} M (e) 10^{-4} M concentrations

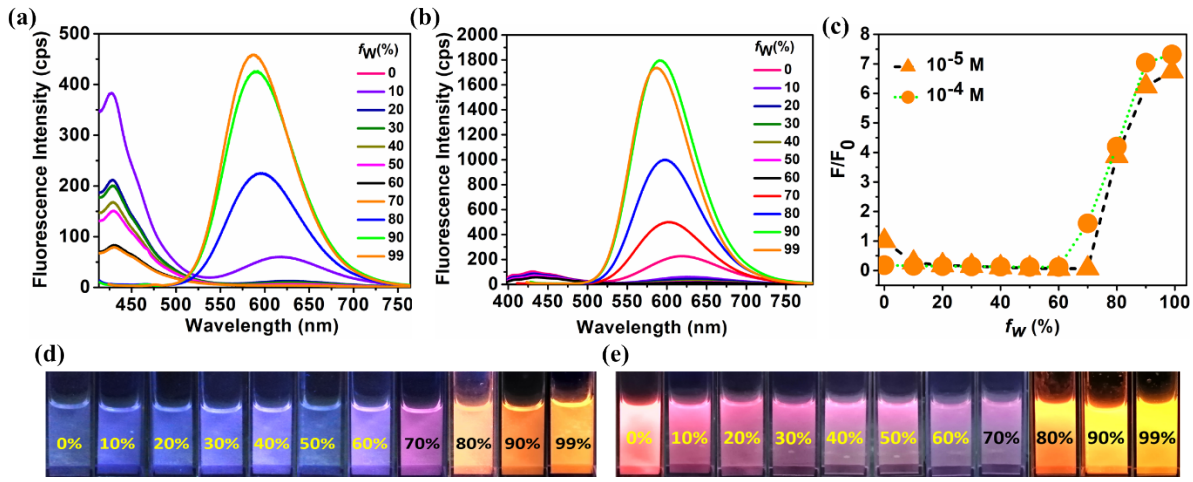

Fig. S27. AIE-property of **PONCN**, emissions with probe concentrations of (a) 10^{-5} M (b) 10^{-4} M (c) F/F_0 vs f_w (%) plot; images captured under UV-365 nm bulb for **PONCN** (d) 10^{-5} M (e) 10^{-4} M concentrations

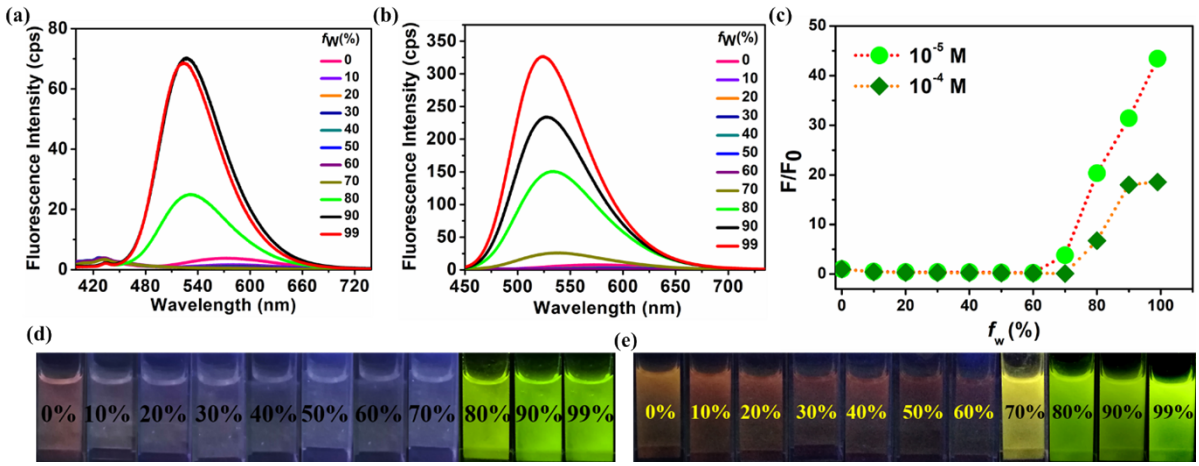

Fig. S28. AIE-property of **OXNCN**,[1] emissions with probe concentrations of (a) 10^{-5} M (b) 10^{-4} M (c) F/F_0 vs f_w (%) plot; images captured under UV-365 nm bulb for **OXNCN** (d) 10^{-5} M (e) 10^{-4} M concentrations

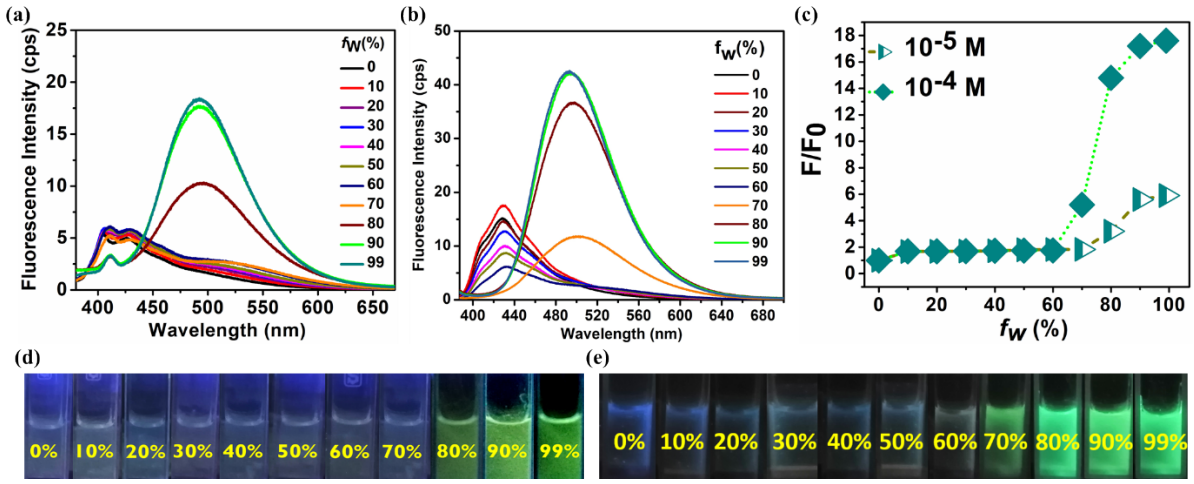

Fig. S29. AIE-property of **DBTNCN**, emissions with probe concentrations of (a) 10^{-5} M (b) 10^{-4} M (c) F/F_0 vs f_w (%) plot; images captured under UV-365 nm bulb for **DBTNCN** (d) 10^{-5} M (e) 10^{-4} M concentrations

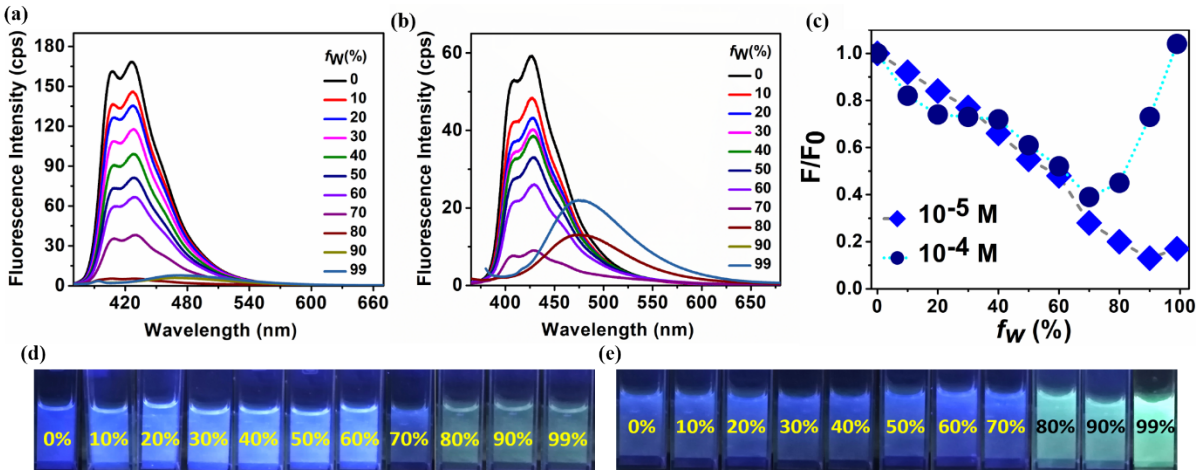

Fig. S30. AIE-property of **DBFNCN**, emissions with probe concentrations of (a) 10^{-5} M (b) 10^{-4} M, (c) F/F_0 vs f_w (%) plot; images captured under UV-365 nm bulb for **DBFNCN** (d) 10^{-5} M (e) 10^{-4} M concentrations.

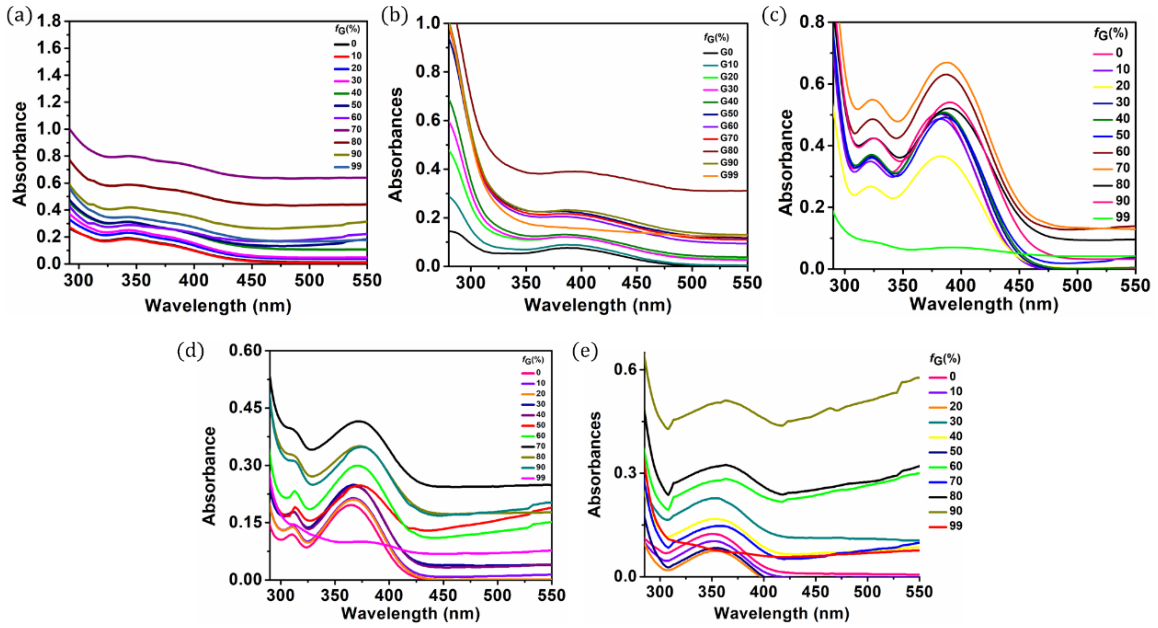

Fig. S31. Absorbance shifts for viscosity-induced emission for the synthesized compounds

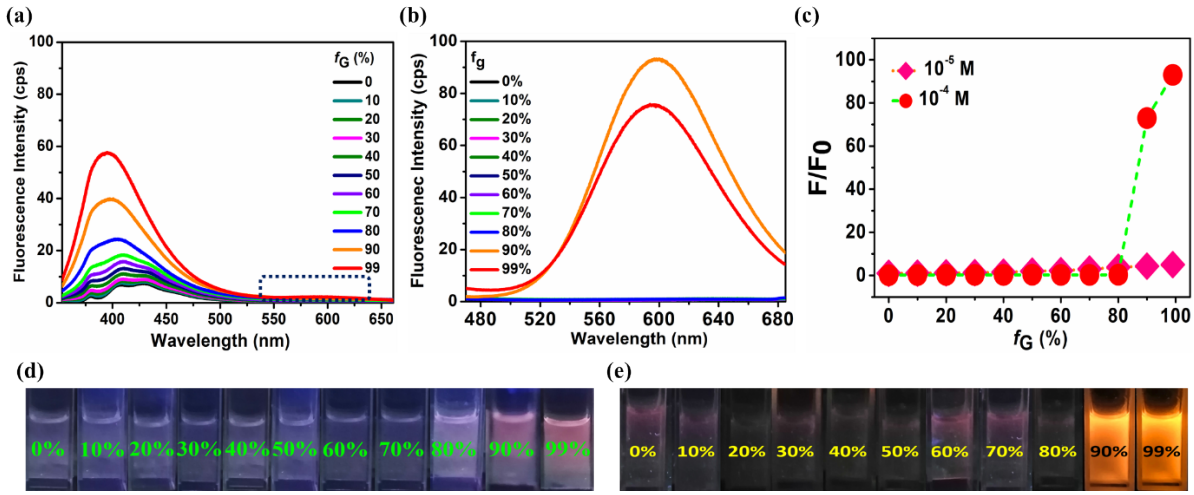

Fig. S32. VIE-property of **TANCN**, emissions with probe concentrations of (a) 10^{-5} M (b) 10^{-4} M (c) F/F_0 vs f_w (%) plot [f_G (%) is the added glycerol fraction, F_0 is the emission intensity at f_G (%) = 0, and F is the emission intensity for the VIE effect at certain f_G (%)]; images captured under UV-365 nm bulb for **TANCN** (d) 10^{-5} M (e) 10^{-4} M concentrations

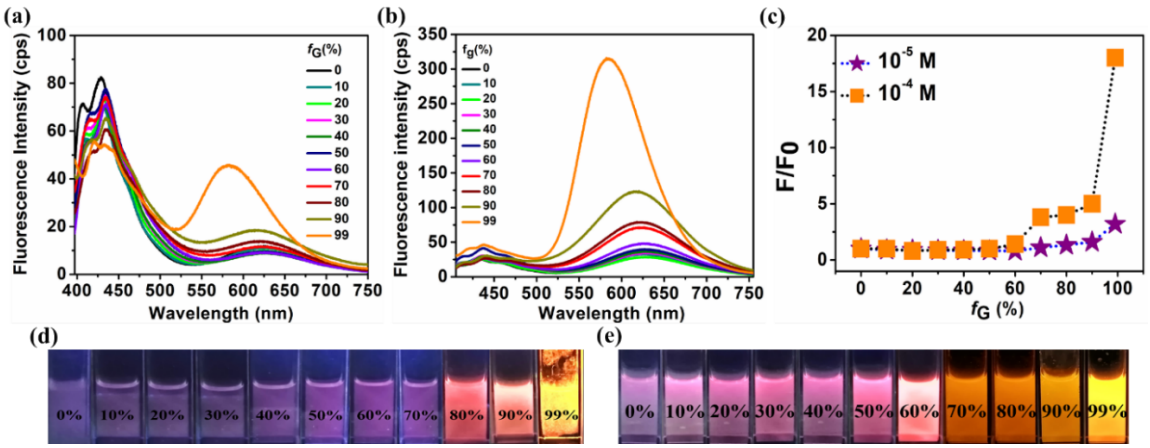

Fig. S33. VIE-property of **PONCN**, emissions with probe concentrations of (a) 10^{-5} M (b) 10^{-4} M (c) F/F_0 vs f_w (%) plot; images captured under UV-365 nm bulb for **TANCN** (d) 10^{-5} M (e) 10^{-4} M concentrations

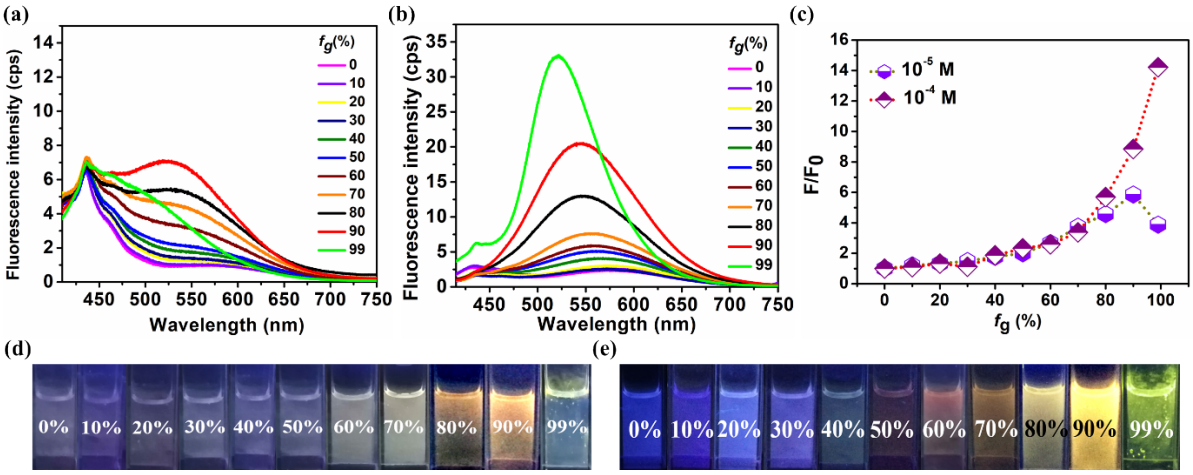

Fig. S34. VIE-property of **OXNCN**, emissions with probe concentrations of (a) 10^{-5} M (b) 10^{-4} M (c) F/F_0 vs f_w (%) plot; images captured under UV-365 nm bulb for **TANCN** (d) 10^{-5} M (e) 10^{-4} M concentrations

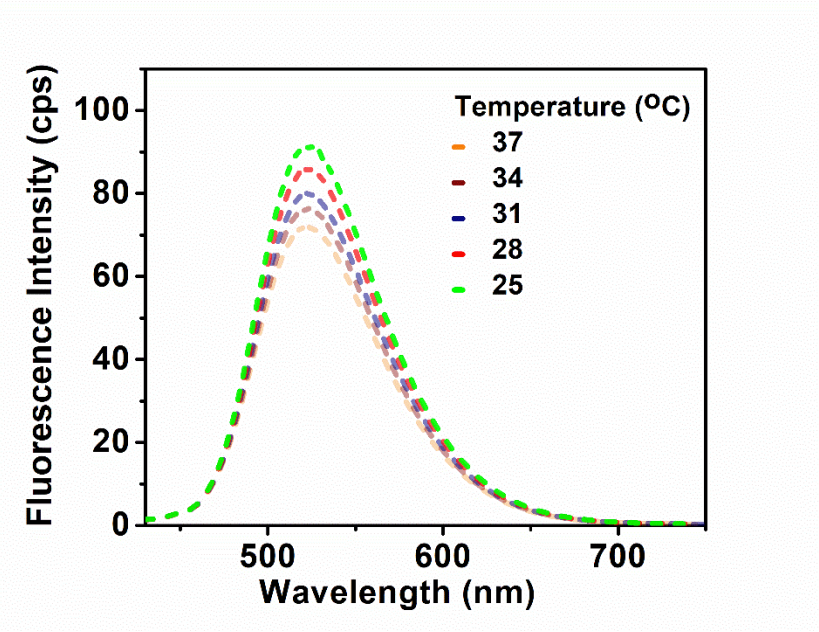

Fig. S35. Temperature-dependent emission from **OXNCN** (10^{-5} M) in PBS

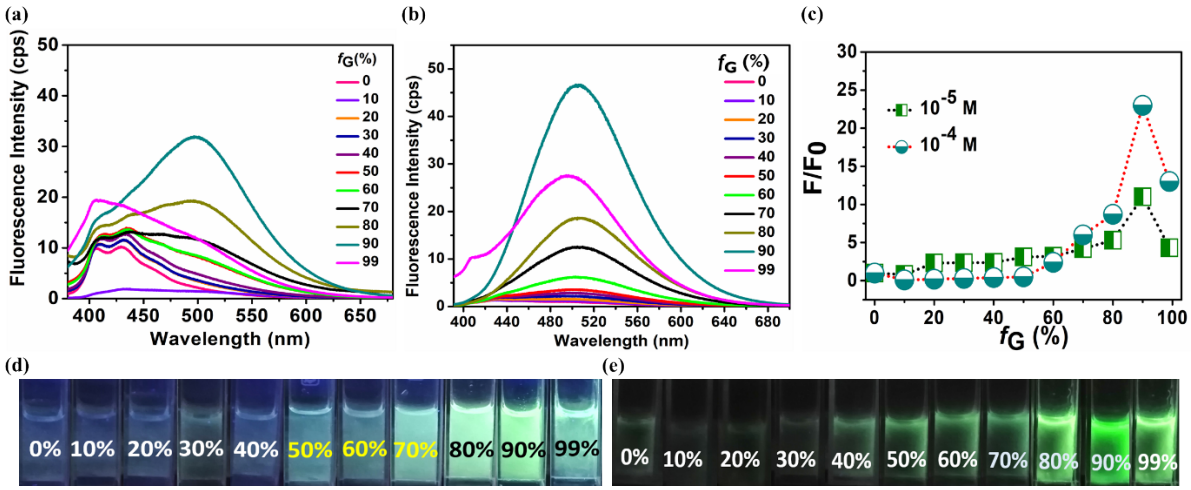

Fig. S36. VIE-property of **DBTNCN**, emissions with probe concentrations of (a) 10^{-5} M (b) 10^{-4} M (c) F/F_0 vs f_w (%) plot; images captured under UV-365 nm bulb for **DBTNCN** (d) 10^{-5} M (e) 10^{-4} M concentrations

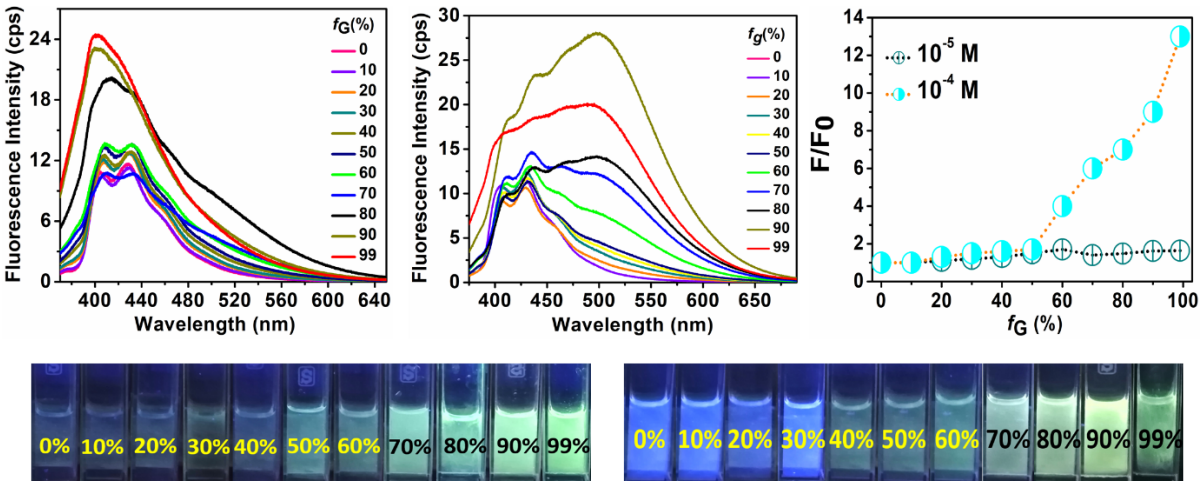

Fig. S37. VIE-property of **DBFNCN**, emissions with probe concentrations of (a) 10^{-5} M (b) 10^{-4} M (c) F/F_0 vs f_w (%) plot; images captured under UV-365 nm bulb for **DBFNCN** (d) 10^{-5} M (e) 10^{-4} M concentrations

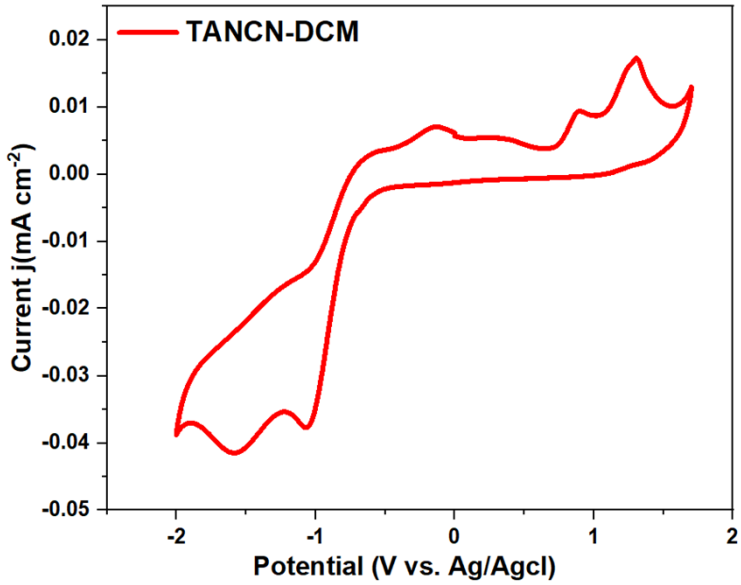

Fig. S38. HOMO-LUMO calculation from CV for **TANCN** in DCM

E_{HOMO} (DCM) = - (E^{OX}_{Onset} - 0.49 + 4.8) eV = - (1.1063- 0.49 + 4.8) eV = -5.4163 eV

E_{LUMO} (DCM) = - (E^{Red}_{Onset}- 0.49 + 4.8) eV = - (-1.2510- 0.49 + 4.8) eV = -3.059 eV

Energy Gap (Eg) = E_{LUMO}- E_{HOMO} = (-3.059 + 5.4163) eV = 2.3573 eV

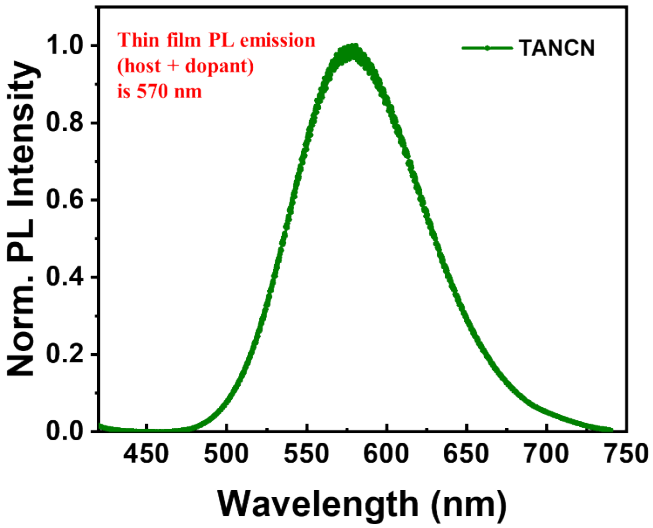

Fig. S39. Thin film PL emission for for 30 wt.% **TANCN: CBP**

NMR Spectra:

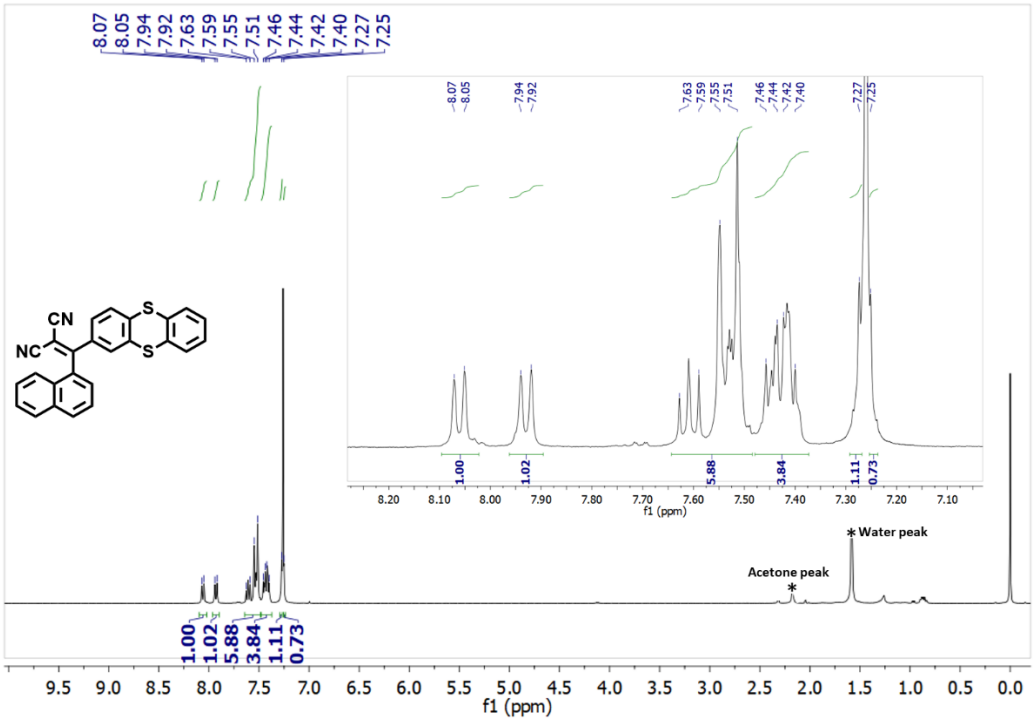

Figure S40. [1]H NMR spectra for 2-(naphthalen-1-yl(thianthren-2-yl)methylene)malononitrile[1]

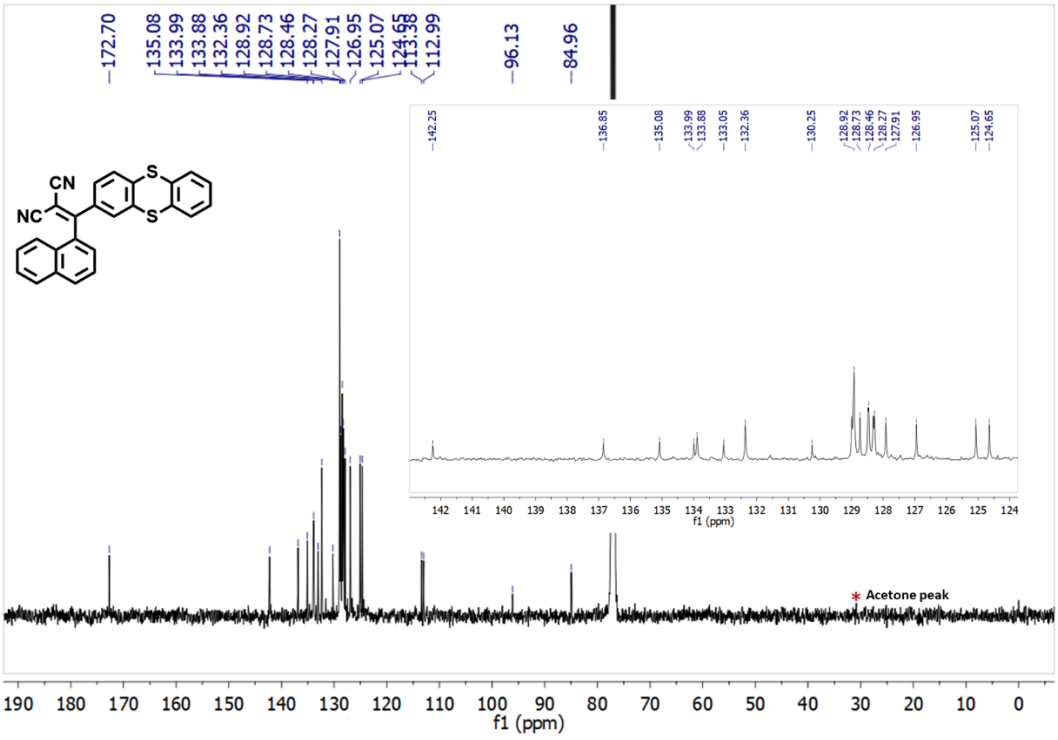

Figure S41. ^{13}C NMR spectra for 2-(naphthalen-1-yl(thianthren-2-yl)methylene)malononitrile[1]

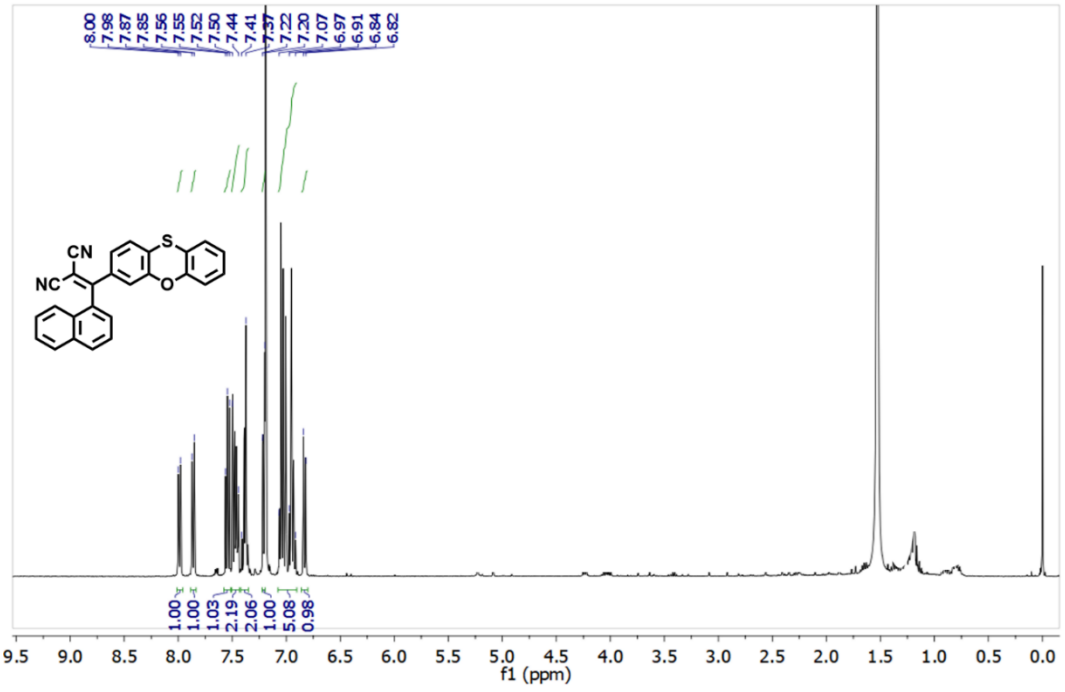

Figure S42. ^{1}H NMR spectra for 2-(naphthalen-1-yl(phenoxathiin-3-yl)methylene)malononitrile[1]

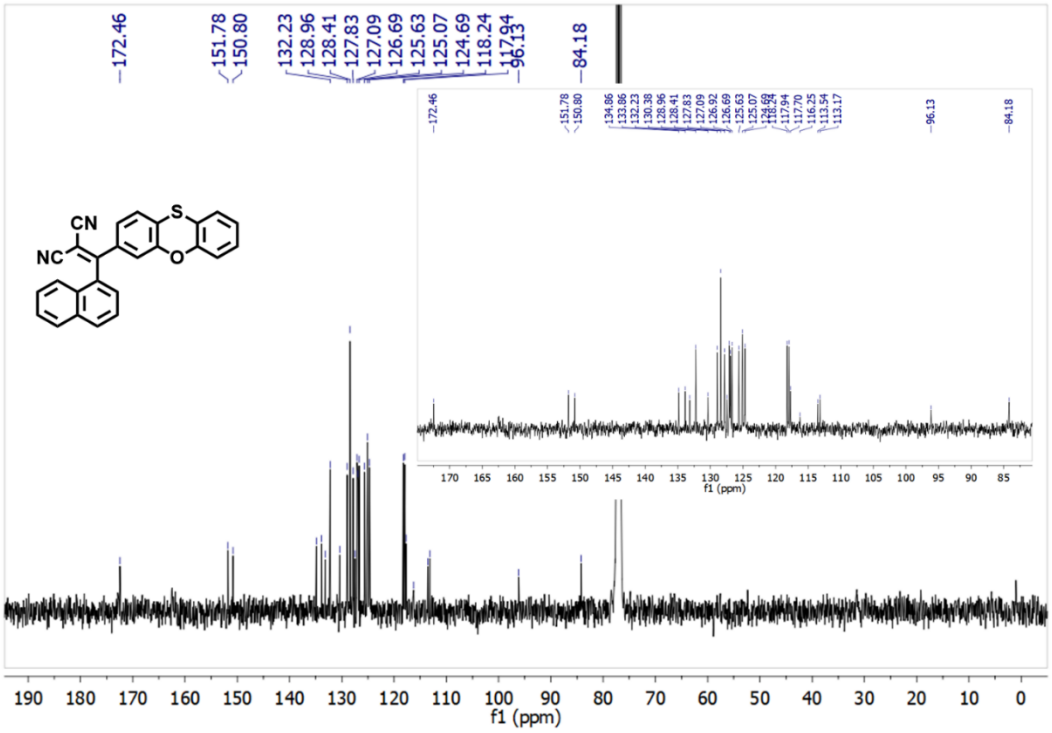

Figure S43. ^{13}C NMR spectra for 2-(naphthalen-1-yl(phenoxathiin-3-yl)methylene)malononitrile[1]

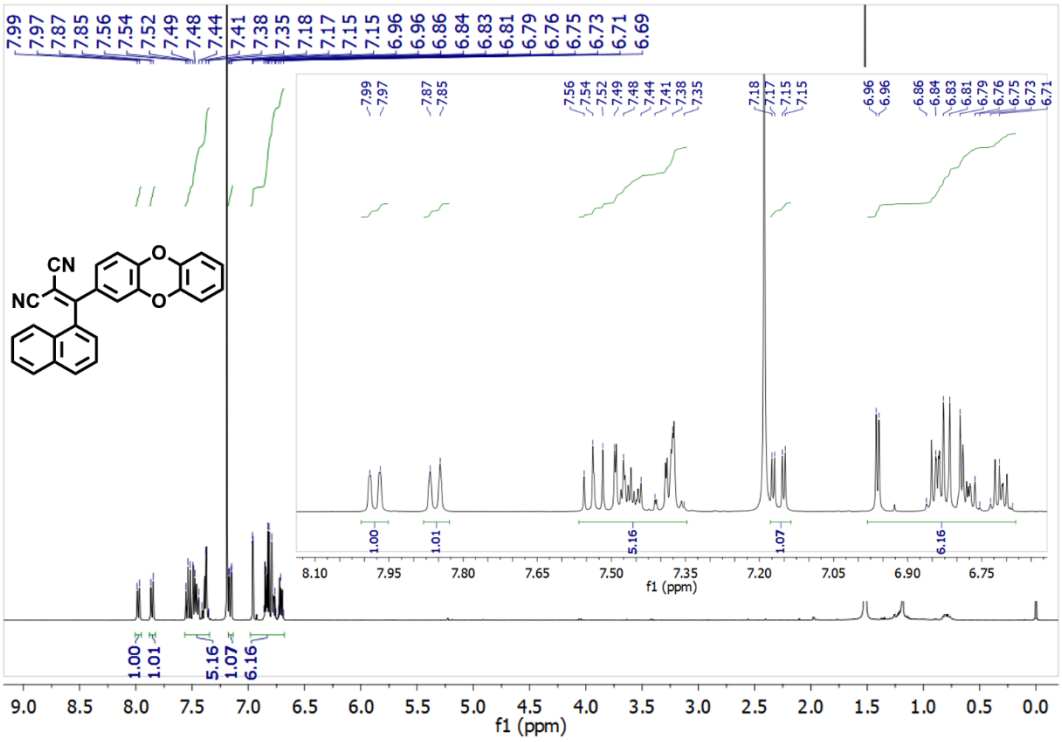

Figure S44. ^{1}H NMR spectra for 2-(dibenzo[b,e][1,4]dioxin-2-yl(naphthalen-1-yl)methylene)malononitrile)[1]

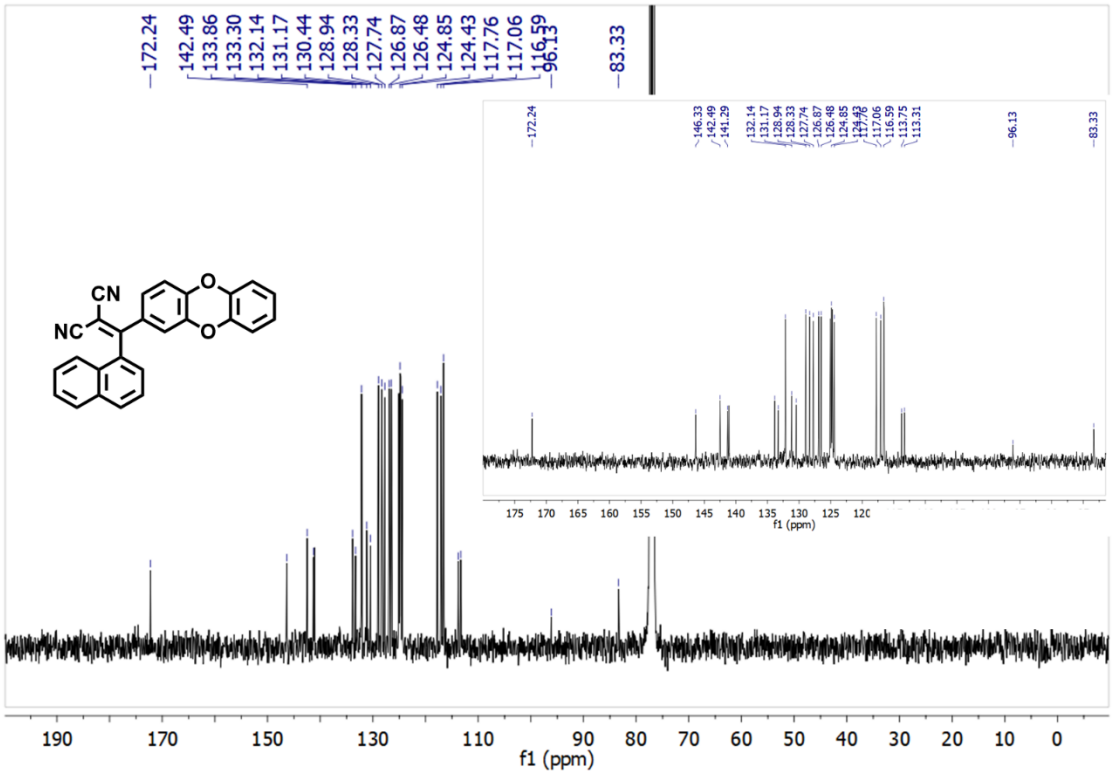

Figure S45. ^{13}C NMR spectra for 2-(dibenzo[b,e][1,4]dioxin-2-yl(naphthalen-1-yl)methylene)malononitrile)[1]

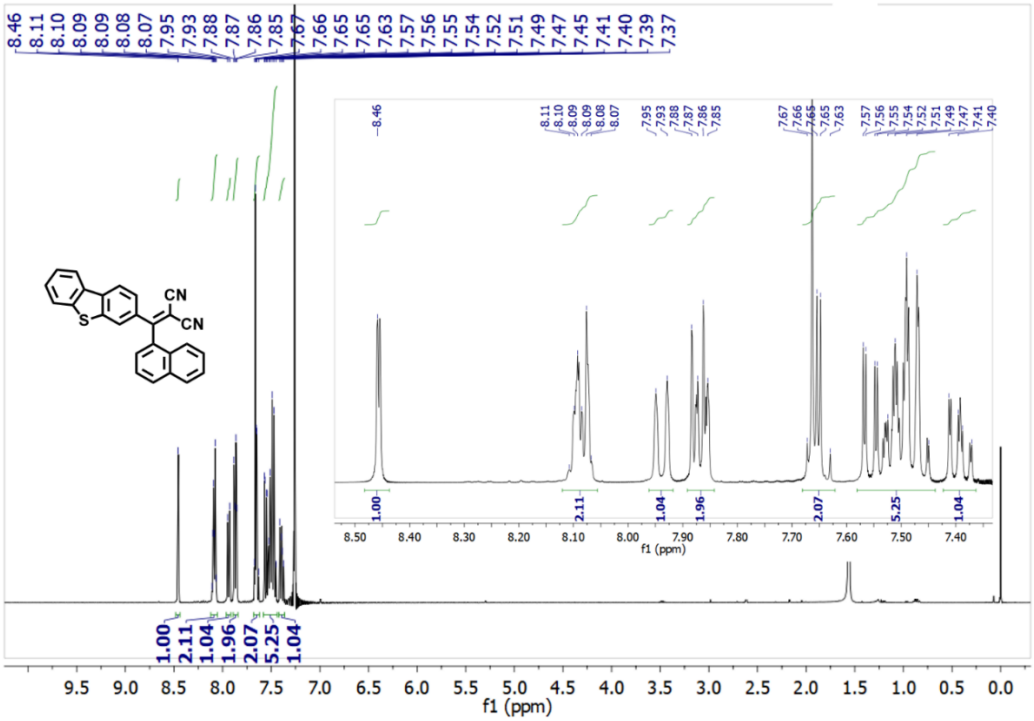

Figure S46. ^{1}H NMR spectra for 2-(dibenzo[b,d]thiophen-3-yl(naphthalen-1-yl)methylene)malononitrile[1]

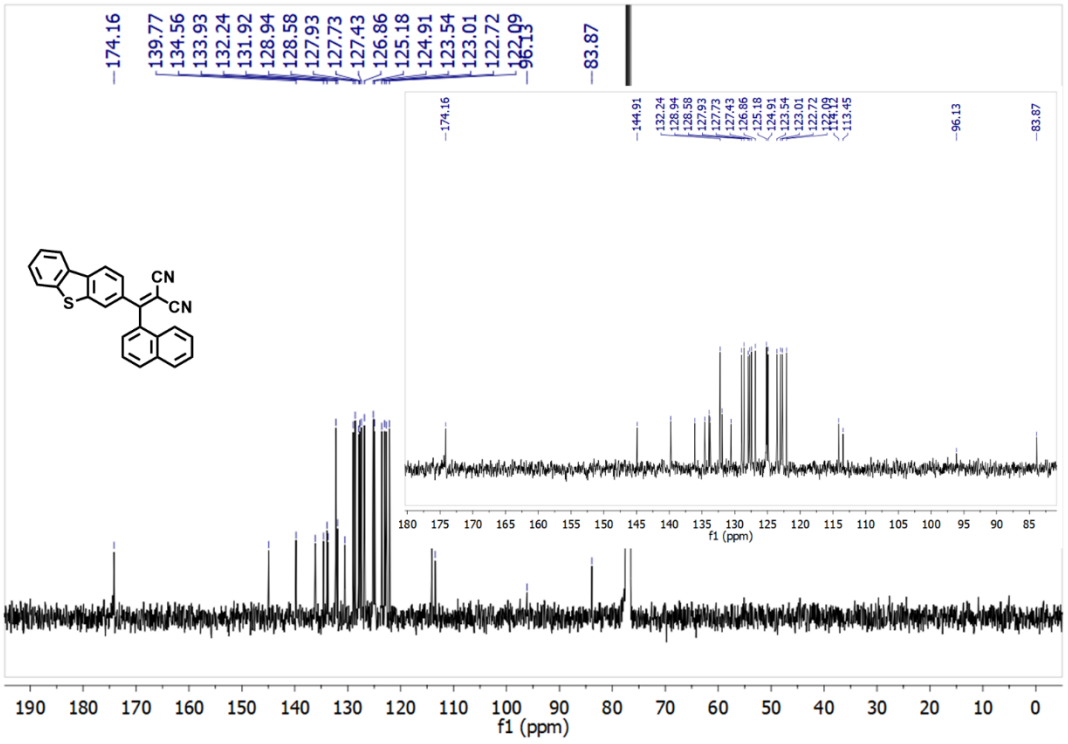

Figure S47. ^{13}C NMR spectra for 2-(dibenzo[b,d]thiophen-3-yl(naphthalen-1-yl)methylene)malononitrile[1]

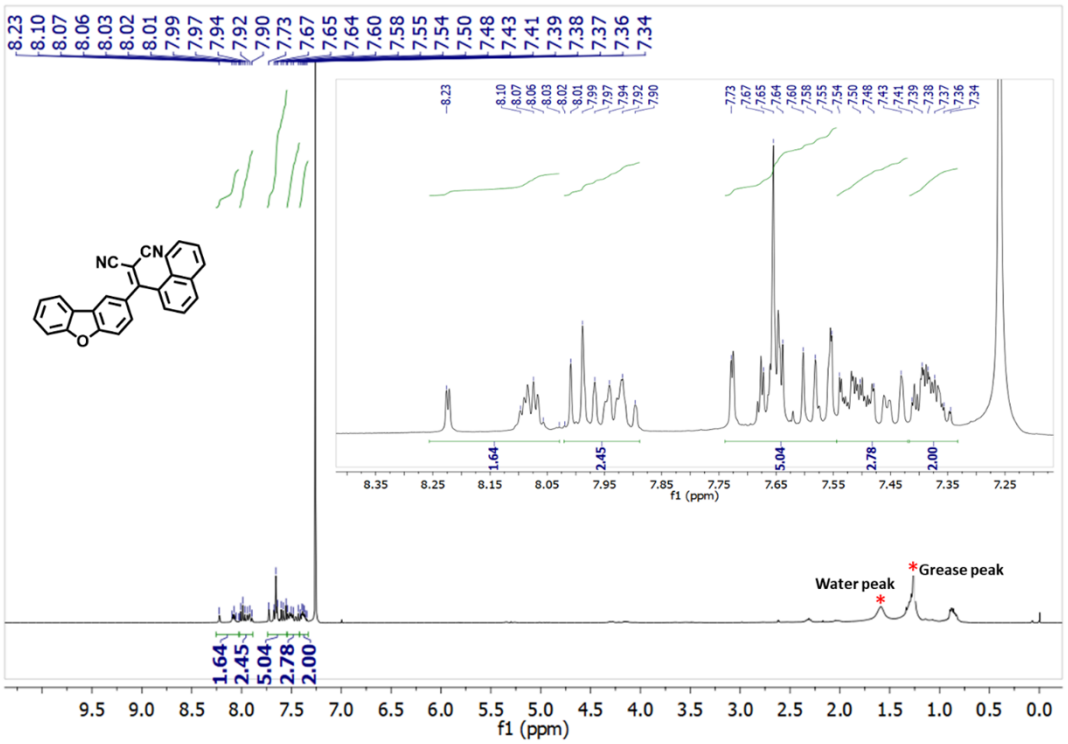

Figure S48. ^{1}H NMR spectra for 2-(dibenzo[b,d]thiophen-3-yl(naphthalen-1-yl)methylene)malononitrile[1]

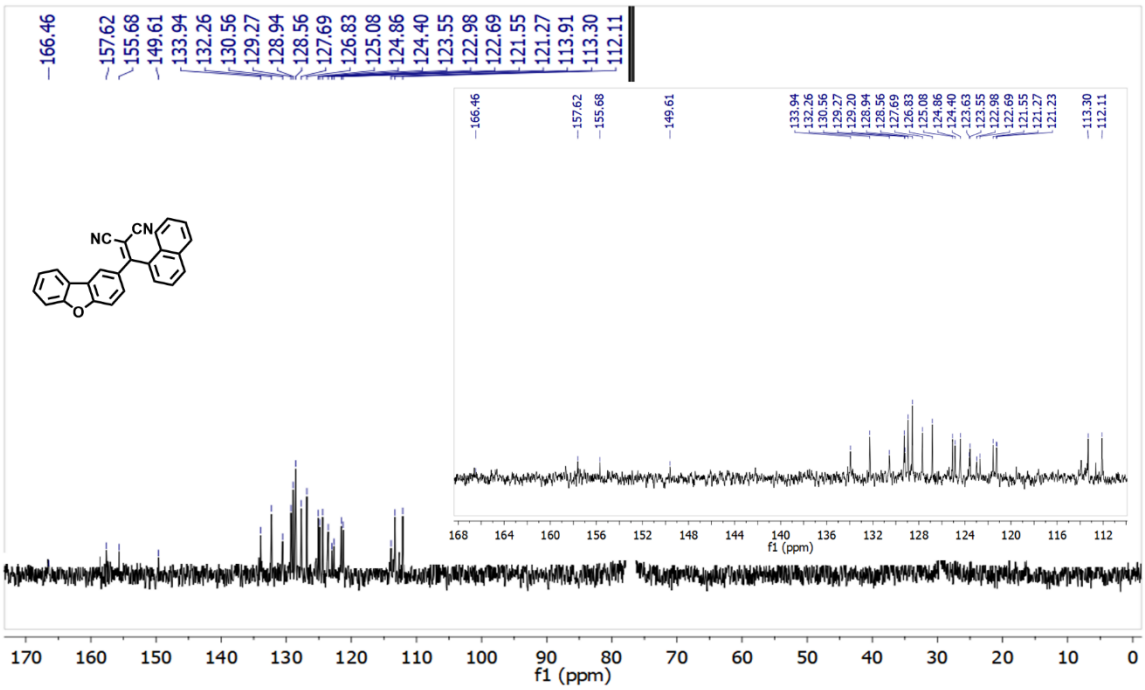

Figure S49. ^{13}C NMR spectra for 2-(dibenzo[b,d]furan-3-yl(naphthalen-1-yl)methylene)malononitrile[1]

Methods and measurements

Steady-state absorption and fluorescence measurements

Solid-state absorption spectra were recorded u sing a JASCO-500 spectrophotometer, and the solution-state absorption spectra were recorded using a UV-vis-NIR spectrophotometer (Hitachi F7000, Japan). Solution-state emission spectra were obtained using an FP-6300 spectrometer (JASCO), and by using a 10 mm path-length quartz cuvette, while the solid-state emission spectra were received using a fluorimeter (Fluorolog, HORIBA). All the emission spectra were obtained at the corresponding absorption wavelengths.

Absolute/relative quantum yield and time-resolved lifetime decay measurement

The absolute quantum yield (Φ_f) values for solid samples were measured using the calibrated integrating sphere method with a fluorimeter (Fluorolog, HORIBA), and absolute errors within ~± 2% have been included while for the relative quantum yield (relative Φ_f) in the solution state, the error is ±5%.

Time-resolved fluorescence measurements were measured using a time-correlated single-photon counting (TCSPC) unit (Horiba Deltaflex). The laser used for all the samples was of 510 nm. All the measurements were undergone at room temperature. The decay fitting was done by keeping the χ^2 value close to 1.

The average lifetime was obtained by fitting the decay profiles to a tri- or bi-exponential function eqn-1. Fit = A1.exp (-t/ τ1) + A2.exp (-t/ τ2) + A3.exp (-t/ τ3) ……..…….(eq-1)

α1, α 2 are the weighted components and τ1, τ2, τ3 are the individual lifetime components of the decay. The qualities of the fit were understood by judging the chi square (χ2) values. The rate constants are calculated by using: $k_r = [\Phi_f / \tau_{avg}]\ s^{-1}$; $k_{nr} = [1-\Phi_f / \tau_{avg}]\ s^{-1}$

FT-IR spectra

An FT-IR spectrometer (FT/IR-4200, Jasco) was utilized to record the IR spectra of the samples. Solid samples were mixed with KBr to form pellets to record the spectra.

Density functional theory studies

The ground state (S_0) optimized geometries and HOMO-LUMO of all the molecules calculated at B3LYP/6-31G(d) level of theory. All calculations used the polarizable continuum model (PCM); solvation modal for DCM, Hexane and DMF solvents compared with the reported experimental results. The excited states of all the molecules are performed with different functionals B3LYP, and M06-2X)[2]. As a result, excited state (S_1 and T_1) calculations are performed in M06-2X/6-31G(d) level of theory with a time dependent density functional theory (TD-DFT) approach. The calculated results of the total dipole moment and total polarization of solvents using M06-2X/6-31G(d) level of theory.[3] All these calculations are performed in Gaussian 09 package.[4] The electron density and natural transition orbital (NTO) analysis were performed to study the nature of the excited states.[5] Root mean square deviation (RMSD) calculations were done using Kabsch algorithm.[6] All structural and MOs were visualizing using Avogadro software.[7]

Single-crystal X-ray measurement

All measurements were performed on a Rigaku XtaLAB P200 diffractometer using multi-layer mirror monochromated Cu-Ka radiation (λ=1.54184 Å). The data were collected at a temperature of -173 ± 1 °C to a maximum 2θ value of 149.8 and were processed using

CrysAlisPro (Rigaku Oxford Diffraction). The linear absorption coefficient (μ) for Cu-K_α radiation is 18.391 cm^{-1}. An applied empirical absorption correction resulted in transmission factors ranging from 0.227 to 0.593. The data were corrected for the Lorentz and polarization effects. The structure was solved by direct methods (SIR2011) and expanded by Fourier techniques. The non-hydrogen atoms were refined anisotropically whether the hydrogen atoms were refined by the riding model. All the calculations were performed using the Olex2 crystallographic software package except for the refinement, which was done using SHELXL Version 2014/7.[8,9]

Cyclic voltammetry study Procedure and calculation:

The HOMO/LUMO energy levels were calculated from the oxidation onset/reduction potentials in due course of positive/negative scans. For **TANCN**, 10^{-5} M of DCM (dichloromethane) solution was used with glassy carbon (GC) electrode as working electrode (WE) along with the Pt-wire and Ag/AgCl were used as a counter electrode (CE) and reference electrode (RE) respectively with a 0.1 M tetrabutylammonium perchlorate (TBAP) in the respective solvents as an electrolyte in a typical three-electrode system at normal condition.

Device fabrication

The OLEDs were fabricated on indium-tin-oxide (ITO) coated glass substrates, which behave as an anode. The ITO surfaces were cleaned ultrasonically with Hellmanex® III detergent, deionized water, acetone, and isopropanol, respectively. The substrates were dried with N_2 blow and exposed to ultraviolet (UV) ozone cleaner treatment for 20 mins to improve hole injection. After ozone treatment, PEDOT:PSS was spin-coated onto the ITO substrates at a spin speed of 4000 rpm for 60 seconds and annealed at 140 ℃ for 20 min. Following that, PVK solution was prepared in chlorobenzene and spin-coated on top of PEDOT:PSS under 3000 rpm and dried at 130 ℃ for 60 seconds. The emitting layer (30 wt.% TANCN: CBP in toluene) was coated at a spinning speed of 3000 rpm and then all the substrates were loaded in a thermal evaporator for further deposition. Finally, PPT, TmPyPB, Liq and Al were consecutively deposited in a high vacuum at a pressure lower than 10^{-6} torr for thermal deposition. The OLED devices' active area was 4.5 mm^2. The electroluminance measurements were performed at ambient conditions using a Keithley 2450 source meter, which is connected to a silicon photodetector. The external quantum efficiency (EQE) values were calculated from the electroluminance spectra, assuming the Lambertian emission profile.

REFERENCES:

1 S. Bhuin, P. Chakraborty, P. Yogeeswari and M. Chakravarty, *ACS Appl. Bio Mater.*, 2025. [DOI: 10.1021/acsabm.4c01817]

2 Y. Zhao, D. G. Truhlar, *Theor. Chem. Acc.*, 2008, **119**, (5–6), 525.

3 P. K. Samanta, M. M. Alam, R. Misra, S. K. Pati , *Phys. Chem. Chem. Phys*., 2019, **21**, 17343-17355.

4 M. J. Frisch, G. W. Trucks, H. B. Schlegel, G. E. Scuseria, M. A. Robb, J. R. Cheeseman, G. Scalmani, V. Barone, G. A. Petersson, H. Nakatsuji, Gaussian 09, Revision D.01. Gaussian, Inc., Wallingford CT 2013.

5 R. L. Martin, Natural Transition Orbitals. *J. Chem. Phys.*, 2003, **118** (11), 4775–4777.

6 W. Kabsch, *Acta Crystallographica*, 1976 A32:922-923. (Code: https://github.com/charnley/rmsd)

7 M. D. Hanwell, D. E. Curtis, D. C. Lonie, D.C., *J CheminformI*, 2012, **4**, 17.

8 CrysAlisPro 1.171.40.67a, (Rigaku OD, 2019).

9 G. M. Sheldrick, *Acta Crystallogr., Sect. A: Found. Crystallogr*. 2008, **64**, 112.
